

Global- and regional-scale hydrological response to early Eocene warmth

Margot Cramwinckel¹, Natalie J Burls², Abdullah A Fahad², Scott Knapp², Christopher K West³, Tammo Reichgelt⁴, David R Greenwood⁵, Wing-Le Chan⁶, Yannick Donnadieu⁷, David Hutchinson⁸, Agatha Margaretha De Boer⁹, Jean-Baptiste Ladant¹⁰, Polina Morozova¹¹, Igor Niezgodzki¹², Gregor Knorr¹³, Sebastian Steinig¹⁴, Zhongshi Zhang¹⁵, Jiang Zhu¹⁶, Ran Feng⁴, Daniel J. Lunt¹⁴, Ayako Abe-Ouchi⁶, and Gordon N. Inglis¹⁷

¹Utrecht University

²George Mason University

³University of Alberta

⁴University of Connecticut

⁵Brandon University

⁶University of Tokyo

⁷Centre national de la recherche scientifique

⁸University of New South Wales

⁹Stockholm University

¹⁰Laboratoire des Sciences du Climat et de l'Environnement

¹¹Skolkovo Institute of Science and Technology

¹²ING PAN - Institute of Geological Sciences Polish Academy of Sciences

¹³AWI Bremerhaven

¹⁴University of Bristol

¹⁵Bjerknes Centre for Climate Research

¹⁶National Center for Atmospheric Research

¹⁷University of Southampton

November 23, 2022

Abstract

Earth's hydrological cycle is expected to intensify in response to global warming, with a 'wet-gets-wetter, dry-gets-drier' response anticipated. The subtropics ($\sim 15\text{-}30^\circ\text{N/S}$) are predicted to become drier, yet proxy evidence from past warm climates suggests these regions may be characterised by wetter conditions. Here we use an integrated data-modelling approach to reconstruct global- and regional-scale rainfall patterns during the early Eocene ($\sim 48\text{-}56$ million years ago), with an emphasis on the subtropics. Model-derived precipitation–evaporation ($P-E$) estimates in the tropics ($0\text{-}15^\circ\text{N/S}$) and high latitudes ($>60^\circ\text{N/S}$) are positive and increase in response to higher temperatures, whereas model-derived $P-E$ estimates in the subtropics ($15\text{-}30^\circ\text{N/S}$) are negative and decrease in response to higher temperatures. This is consistent with a 'wet-gets-wetter, dry-gets-drier' response. However, some DeepMIP model simulations predict increasing – rather than decreasing – subtropical precipitation at higher temperatures (e.g., CESM, GFDL). Using moisture budget diagnostics we find that the models with higher subtropical precipitation are characterised by a reduction in the strength of subtropical moisture circulation due to weaker meridional temperature gradients. These model simulations (e.g., CESM, GFDL) agree more closely with various proxy-derived climate metrics and imply a reduction in the strength of subtropical moisture circulation during the early Eocene. Although this was

insufficient to induce subtropical wetting, if the meridional temperature was weaker than suggested by the DeepMIP models, this may have led to wetter subtropics. This highlights the important role of the meridional temperature gradient when predicting past (and future) rainfall patterns.



Paleoceanography & Paleoclimatology

Supporting Information for

Global- and regional-scale hydrological response to early Eocene warmth

Margot J. Cramwinckel^{1,#}, Natalie J. Burls², Abdullah A. Fahad^{2,3}, Scott Knapp², Christopher K. West^{4,5,&}, Tammo Reichgelt⁶, David R. Greenwood⁷, Wing-Le Chan⁸, Yannick Donnadieu⁹, David K. Hutchinson¹⁰, Agatha M. de Boer¹⁰, Jean-Baptiste Ladant¹¹, Polina A. Morozova¹², Igor Niezgodzki¹³, Gregor Knorr¹⁴, Sebastian Steinig¹⁵, Zhongshi Zhang¹⁶, Jiang Zhu¹⁷, Ran Feng¹⁷, Daniel J. Lunt¹⁵, Ayako Abe-Ouchi⁸, and Gordon N. Inglis^{1*}

¹School of Ocean and Earth Science, University of Southampton, Southampton, United Kingdom

²Department of Atmospheric, Oceanic and Earth Sciences, Center for Ocean-Land-Atmosphere Studies, George Mason University, Fairfax, USA

³GMAO, NASA Goddard Space Flight Center, Greenbelt, MD, USA

⁴Department of Earth and Atmospheric Sciences, University of Alberta, Edmonton, Canada

⁵Royal Tyrrell Museum of Palaeontology, Drumheller, Alberta, Canada

⁶Department of Geosciences, University of Connecticut, Storrs, USA

⁷Department of Biology, Brandon University, Brandon, Canada

⁸Atmosphere and Ocean Research Institute, University of Tokyo, Japan

⁹Laboratoire des Sciences du Climat et de l'Environnement, France

¹⁰Department of Geological Sciences, Stockholm University, Sweden

¹¹Earth and Environmental Sciences, University of Michigan, US

¹²Institute of Geography, Russian Academy of Sciences, Russia

¹³Polish Academy of Sciences, Poland

¹⁴Alfred Wegener Institute for Polar and Marine Research, Germany

¹⁵ School of Geographical Sciences, University of Bristol, UK

¹⁶Bjerknes Centre for Climate Research, University of Bergen, Norway

¹⁷National Center For Atmospheric Research, USA

#Now at: Department of Earth Sciences, Utrecht University, Utrecht, The Netherlands

&Now at: Royal Tyrrell Museum of Palaeontology, Alberta, Canada

Contents of this file

Figures S1 to S8 Tables S1 Dataset S1

Introduction

Included are various supplementary figures (S1 to S11), a supplementary table that provides summary statistics for the late Paleocene – early Eocene (LPEE) mean annual precipitation (MAP) proxy compilation (Table S1), and supplementary datasets (Dataset S1).

Supplementary Figures

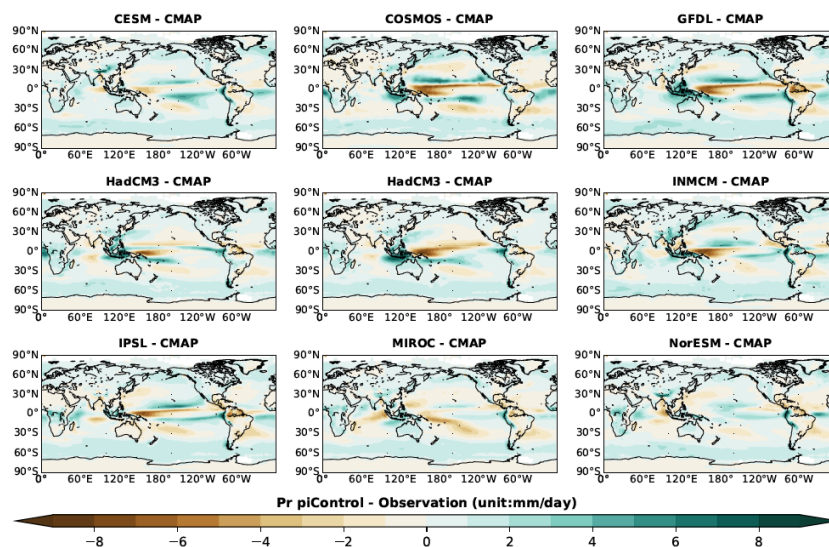


Figure S1 . Precipitation anomalies (mm/day) for the pre-industrial control runs minus modern observations for the 9 models in the DeepMIP ensemble, highlighting model-specific biases in reproducing modern observations.

Hosted file

image3.emf available at <https://authorea.com/users/543996/articles/601477-global-and-regional-scale-hydrological-response-to-early-eocene-warmth>

Figure S2. Temperature anomalies (mm/day) of the DeepMIP experiments, relative to pre-industrial control simulations, ordered by CO₂ forcing and model.

Hosted file

image4.emf available at <https://authorea.com/users/543996/articles/601477-global-and-regional-scale-hydrological-response-to-early-eocene-warmth>

Figure S3. Precipitation anomalies (mm/day) of the DeepMIP experiments, relative to pre-industrial control simulations, ordered by CO₂ forcing and model.

Hosted file

image5.emf available at <https://authorea.com/users/543996/articles/601477-global-and-regional-scale-hydrological-response-to-early-eocene-warmth>

Figure S4. Evaporation anomalies (mm/day) of the DeepMIP experiments, relative to pre-industrial control simulations, ordered by CO₂ forcing and model.

Hosted file

image6.emf available at <https://authorea.com/users/543996/articles/601477-global-and-regional-scale-hydrological-response-to-early-eocene-warmth>

Figure S5. Precipitation minus evaporation (PE; mm/day) anomalies of the DeepMIP experiments, relative to pre-industrial control simulations, ordered by CO₂ forcing and model.

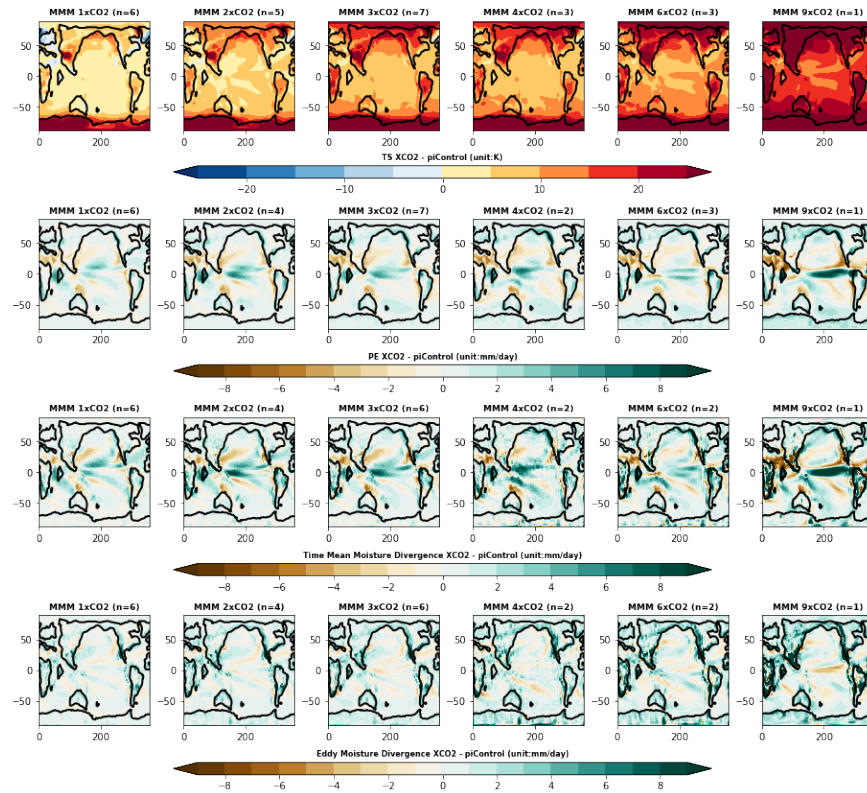


Figure S6 . Spatial patterns of temperature, precipitation, and moisture divergence in the DeepMIP simulations . a) surface air temperature (°C), b) precipitation (mm/day), c) time mean moisture divergence (P-E; mm/day) and d) eddy moisture divergence (P-E; mm/day). "n" values above each plot represent the number of models available for calculating the MMM.

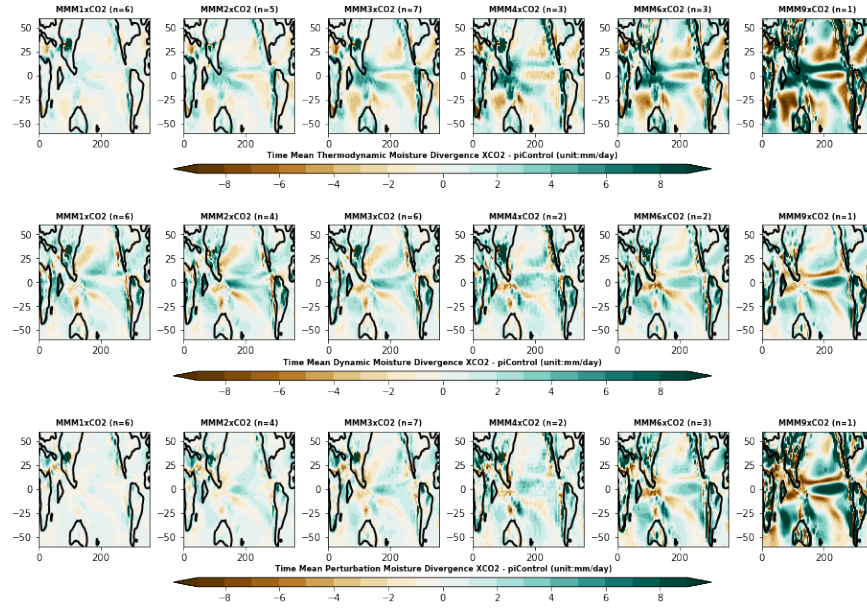


Figure S7 . *Spatial patterns of moisture divergence in the DeepMIP simulations a) time mean moisture divergence associated with thermodynamical changes (P-E; mm/day), b) time mean moisture divergence associated with dynamical changes (P-E; mm/day), c) time mean moisture divergence (P-E; mm/day), "n" values above each plot represent the number of models available for calculating the MMM.*

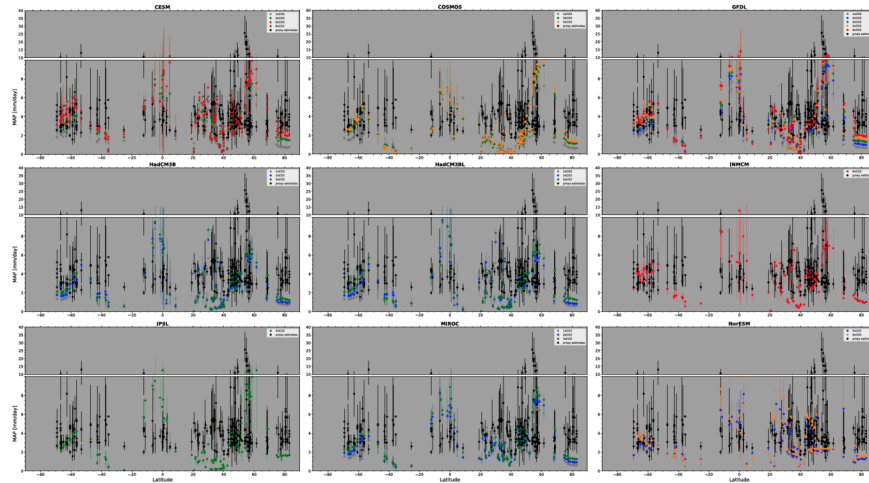


Figure S8 . *Zonal plot proxy-model biases for all of the models in the DeepMIP ensemble. Mean annual precipitation (MAP; mm/day) on the vertical axis (note vertical axis scale break) against latitude on the horizontal axis. Simulations ordered per model (panels), with different CO₂ levels as different colors. Proxy-based data compiled in this study in black. Paleolatitude of 55 Ma used.*

Supplementary Tables

Table S1. Summary statistics of our late Paleocene – early Eocene (LPEE) mean annual precipitation (MAP) proxy compilation

	Number of data points in compilation (total = 322)	Number of data points (%)
Time period	n =	%
general "LPEE"	33	10%
Thanetian	40	12%
PETM	6	2%
Ypresian	197	61%
Lutetian	46	14%
Proxy type	n =	%
LP; CLAMP	45	14%
LP; LAA	84	26%
NLR	51	16%
NLR; BA	50	16%
NLR; CA	87	27%
NLR; CAM	3	1%
WP	2	1%
Continent / Ocean	n =	%
Africa	11	3%
Antarctica	25	8%
Arctic Ocean	6	2%
Asia	75	23%
New Zealand and Australia	46	14%
Europe	7	2%
North America	129	40%
South America	23	7%
Paleolatitude band (hotspot reference frame)	n =	%
60-90S	41	13%
30-60S	47	15%
15-30S	1	0%
0-15S	12	4%
0-15N	14	4%
15-30N	16	5%
30-60N	142	44%
60-90N	49	15%

Hosted file

essoar.10512308.1.docx available at <https://authorea.com/users/543996/articles/601477-global-and-regional-scale-hydrological-response-to-early-eocene-warmth>

Margot J. Cramwinckel^{1,#}, Natalie J. Burls², Abdullah A. Fahad^{2,3}, Scott Knapp², Christopher K. West^{4,5,&}, Tammo Reichgelt⁶, David R. Greenwood⁷, Wing-Le Chan⁸, Yannick Donnadieu⁹, David K. Hutchinson¹⁰, Agatha M. de Boer¹⁰, Jean-Baptiste Ladant¹¹, Polina A. Morozova¹², Igor Niezgodzki¹³, Gregor Knorr¹⁴, Sebastian Steinig¹⁵, Zhongshi Zhang¹⁶, Jiang Zhu¹⁷, Ran Feng¹⁷, Daniel J. Lunt¹⁵, Ayako Abe-Ouchi⁸, and Gordon N. Inglis^{1*}

¹School of Ocean and Earth Science, University of Southampton, Southampton, United Kingdom

²Department of Atmospheric, Oceanic and Earth Sciences, Center for Ocean-Land-Atmosphere Studies, George Mason University, Fairfax, USA

³GMAO, NASA Goddard Space Flight Center, Greenbelt, MD, USA

⁴Department of Earth and Atmospheric Sciences, University of Alberta, Edmonton, Canada

⁵Royal Tyrrell Museum of Palaeontology, Drumheller, Alberta, Canada

⁶Department of Geosciences, University of Connecticut, Storrs, USA

⁷Department of Biology, Brandon University, Brandon, Canada

⁸Atmosphere and Ocean Research Institute, University of Tokyo, Japan

⁹Laboratoire des Sciences du Climat et de l'Environnement, France

¹⁰Department of Geological Sciences, Stockholm University, Sweden

¹¹Earth and Environmental Sciences, University of Michigan, US

¹²Institute of Geography, Russian Academy of Sciences, Russia

¹³Polish Academy of Sciences, Poland

¹⁴Alfred Wegener Institute for Polar and Marine Research, Germany

¹⁵ School of Geographical Sciences, University of Bristol, UK

¹⁶Bjerknes Centre for Climate Research, University of Bergen, Norway

¹⁷National Center For Atmospheric Research, USA

[#]Now at: Department of Earth Sciences, Utrecht University, Utrecht, The Netherlands

[&]Now at: Royal Tyrrell Museum of Palaeontology, Alberta, Canada

^{*}Corresponding author. Email: gordon.inglis@soton.ac.uk

Abstract

Earth’s hydrological cycle is expected to intensify in response to global warming, with a ‘wet-gets-wetter, dry-gets-drier’ response anticipated. The subtropics ($\sim 15\text{-}30^\circ\text{N/S}$) are predicted to become drier, yet proxy evidence from past warm climates suggests these regions may be characterised by wetter conditions. Here we use an integrated data-modelling approach to reconstruct global- and regional-scale rainfall patterns during the early Eocene ($\sim 48\text{-}56$ million years ago), with an emphasis on the subtropics. Model-derived precipitation–evaporation ($P\text{-}E$) estimates in the tropics ($0\text{-}15^\circ\text{N/S}$) and high latitudes ($>60^\circ\text{N/S}$) are positive and increase in response to higher temperatures, whereas model-derived $P\text{-}E$ estimates in the subtropics ($15\text{-}30^\circ\text{N/S}$) are negative and decrease in response to higher temperatures. This is consistent with a ‘wet-gets-wetter, dry-gets-drier’ response. However, some DeepMIP model simulations predict increasing – rather than decreasing – subtropical precipitation at higher temperatures (e.g., CESM, GFDL). Using moisture budget diagnostics we find that the models with higher subtropical precipitation are characterised by a reduction in the strength of subtropical moisture circulation due to weaker meridional temperature gradients. These model simulations (e.g., CESM, GFDL) agree more closely with various proxy-derived climate metrics and imply a reduction in the strength of subtropical moisture circulation during the early Eocene. Although this was insufficient to induce subtropical wetting, if the meridional temperature was weaker than suggested by the DeepMIP models, this may have led to wetter subtropics. This highlights the important role of the meridional temperature gradient when predicting past (and future) rainfall patterns.

Key points:

- The early Eocene hydrological cycle is characterised by a ‘wet-gets-wetter, dry-gets-drier’ response
- The early Eocene exhibits weaker subtropical moisture circulation in simulations with reduced meridional temperature gradients
- This highlights the important role of the meridional temperature gradient when predicting past (and future) rainfall patterns

Introduction

Global warming is projected to be associated with increasing global mean annual precipitation (MAP) and a shift in regional and seasonal rainfall patterns (Masson-Delmotte et al., 2022), with important consequences for societies and ecosystems. Under higher global temperatures, Earth’s atmosphere will contain more water vapour following the Clausius–Clapeyron relation (Held and Soden, 2006). This ‘thermodynamic effect’ forms the basis for the predicted “wet-

gets-wetter, dry-gets-drier” response under enhanced radiative forcing, whereby the existing spatial patterns in precipitation-evaporation ($P-E$) are exacerbated (Held and Soden, 2006; Seager et al., 2010). General circulation models (GCMs) used in Coupled Model Intercomparison Project Phase 6 (CMIP6) suggest that higher global mean surface temperatures (GMST) will lead to wetter high latitudes ($> 60^\circ\text{N/S}$) (i.e., positive $P-E$ change), and drier subtropics ($15-30^\circ\text{N/S}$) (i.e., negative $P-E$ change) (Hoegh-Guldberg et al., 2018; Masson-Delmotte et al., 2022). However, these same models disagree on the nature of change in much of the remainder of the low to middle latitudes, both over land and ocean (Slingo et al., 2022; Masson-Delmotte et al., 2022), which is a key uncertainty for appropriate climate mitigation and adaptation.

Moreover, evidence from warm intervals in the geological past suggests that the subtropics may get wetter (rather than drier) under warmer conditions, i.e. “dry-gets-wetter”. For example, both the Miocene (23.0 to 5.3 million years ago; Ma) and Pliocene (5.3 to 2.6 Ma) yield proxy evidence for wetter subtropics in southern Australia (Sniderman et al., 2016), North Africa (Hailemichael et al., 2002; Schuster et al., 2009), South America (Carrapa et al., 2019) and South-East Asia (Wang et al., 2019). Burls and Federov (2017) suggest this is due to weaker subtropical moisture divergence. Although the impact of changes in circulation is often considered secondary to changes in atmospheric humidity, the former may be important under certain climate scenarios (e.g., weak latitudinal temperature gradients; LTGs) and may even compensate for an increase in atmospheric humidity (Burls & Fedorov 2017).

Here we focus on the early Eocene (56.0 to 47.8 million years ago; Ma), an interval characterised by higher CO_2 values (> 1000 parts per million) (Anagnostou et al., 2020), higher global mean surface temperature ($10-16^\circ\text{C}$ warmer than pre-industrial) (Inglis et al., 2020) and reduced pole-to-equator LTGs (~ 17 to 22°C) (Cramwinckel et al., 2018; Evans et al., 2018; Gaskell et al., 2022). As such, this is an ideal interval to study how changes in the LTG impact subtropical rainfall patterns. However, there are very few quantitative early Eocene-aged MAP estimates from the subtropics ($15-30^\circ\text{N/S}$) and the hydrological response to warming remains largely unknown. To resolve this, we utilise the recently published state-of-the-art Deep-Time Model Intercomparison Project (DeepMIP) suite of model simulations (Lunt et al., 2021) to explore the global- and regional-scale hydrological response to warming. This is combined with a new proxy compilation to answer the following questions: **i)** Are early Eocene simulations characterised by a ‘wet-gets-wetter, dry-gets-drier’ response, **ii)** How do the simulated thermodynamic (i.e., humidity) and dynamic (i.e. moisture circulation) effects contribute to changes in moisture transport in the subtropics, and **iii)** How well do the DeepMIP models replicate proxy-derived MAP estimates?

Methods

Modelling simulations

We make use of the DeepMIP suite of model simulations, embedded in the sixth phase of the Coupled Model Intercomparison Project (CMIP6; (Eyring et al., 2016)). An extensive description of the standard design of these model experiments is provided in Lunt et al. (2017), and a large-scale overview of results has been presented in Lunt et al. (2021). The main advantage of these simulations over the EoMIP (Eocene Modelling Intercomparison Project) “ensemble of opportunity” employed in earlier work (Carmichael et al., 2016) is that the new DeepMIP simulations have been designed and carried out using internally consistent Eocene boundary conditions (from Herold et al., 2014). Simulations have been run at different atmospheric CO₂ levels – typically $\times 1$, $\times 3$, $\times 6$, and $\times 9$ preindustrial (PI) CO₂, but with a subset of these, or additional atmospheric CO₂ concentrations, chosen by some model groups (see Lunt et al., 2017; Lunt et al., 2021). Different CO₂ experiments are expected to provide comparison targets to climate reconstructions for different key time slices, including the early Eocene Climatic Optimum (EECO; ~ 53.3 – 49.1 Ma), the Paleocene–Eocene Thermal Maximum (PETM; ~ 56 Ma), and the latest Paleocene (i.e., pre-PETM). Pre-industrial simulations ($\times 1$ CO₂) with modern continental configurations have also been performed to assess the influence of non-CO₂ Eocene boundary conditions. Simulations have been performed with eight different models (**Table 1**) and detailed descriptions of the models and simulations are provided in Lunt et al. (2021). To explore regional variations in hydroclimate, we subdivide our data into four latitudinal bands (following Burls and Federov, 2017): **I**) the tropics (0 – 15° N/S), **II**) the subtropics (15 – 30° N/S), **III**) the mid-latitudes (30 – 60° N/S), and **IV**) the high-latitudes ($>60^\circ$ N/S). To further deconvolve the cause of global and regional variations, we perform a moisture budget analysis. The analysed climatologies are based on the last 100 years of each simulation. As different models provided slightly different variables, for some models we were not able to provide analysis of P – E (NorESM), or moisture budget analysis (IPSL, INMCM, and NorESM). We compare observed changes in subtropical hydrology to changes in modelled latitudinal temperature gradient (LTG), here taken as the difference in surface temperature between the mid-latitudes (30 – 60° N/S) and the tropics (15° N– 15° S).

Proxy synthesis

Approach

Fossil leaves and palynomorphs (spores/pollen) can provide quantitative estimates of mean annual precipitation (MAP) in the past. The primary approaches are: I) leaf physiognomy (i.e., leaf shape) (Givnish, 1984; Wolfe, 1993; Wing and Greenwood, 1993; Greenwood, 2007) and II) nearest living relative (NLR)-based approaches (Pross et al., 2000; Greenwood et al., 2003; Pancost et al.,

2013; Suan et al., 2017; West et al., 2020). A multi-proxy approach combining leaf physiognomy and NLR data is generally recommended and mitigates the different uncertainties incorporated by individual approaches (e.g., West et al., 2020).

Methods based on leaf physiognomy utilise the correlation between the architecture of leaves and climatic variables. As leaf size and shape are highly sensitive to moisture availability (Givnish, 1984; Peppe et al., 2011; Spicer et al., 2021), fossil leaf architecture can be related to precipitation using univariate methods such as Leaf Area Analysis (LAA) (Wilf et al., 1998). The Climate Leaf Analysis Multivariate Program (CLAMP) (Wolfe, 1993, 1995) combines multiple leaf traits, including leaf area, leaf shape, and margin state (i.e., toothed or untoothed), to provide estimates of annual and seasonal precipitation (Spicer et al., 2021). Anatomical characteristics of fossil wood can likewise reflect climate variables (Wiemann et al., 1998; Poole and van Bergen, 2006). Although wood anatomy as a climate proxy has not had widespread application in deep time climate compilations, multivariate models of various wood anatomical characters are typically used (e.g., Poole et al., 2005).

Nearest living relative (NLR) approaches are based on the premise that the climatic tolerance of a paleo-vegetation assemblage can be inferred from their presumed extant relatives (e.g., Mosbrugger and Utescher, 1997; Fauquette et al., 1998; Greenwood et al., 2003; Willard et al., 2019; West et al., 2020). These methods can be based on macrofossil (most often leaf fossils but also seeds, fruits, or wood) or microfossil (i.e. sporomorphs) paleobotanical assemblages, as long as the taxa can be correlated to a living relative with a known climatic tolerance. The coexistence approach (CA; Mosbrugger and Utescher, 1997) is a specific instance of this, in which the single climatic interval in which all NLRs can coexist is reconstructed. More recent studies employing Bioclimatic Analysis (BA) typically calculate probability density functions of climatic variables instead of minimum-to-maximum intervals (e.g., Willard et al., 2019; West et al., 2020). The Climatic Amplitude Method (CAM) is an alternative NLR approach that incorporates relative abundances of different taxa (Fauquette et al., 1998).

Proxy compilation

Here we compile paleobotanical MAP estimates for the late Paleocene (59.2 to 56 Ma; Thanetian) to early Eocene (56.0 to 47.8 Ma; Ypresian). Our compilation builds upon previous EECO- (Carmichael et al., 2016) and Paleocene-Eocene Thermal Maximum (PETM; 56 Ma)-aged (Carmichael et al., 2017) compilations. We supplement this with i) published MAP estimates generated since, and ii) newly generated MAP estimates using CLAMP and NLR on published palynological and macrofloral (predominantly leaf-based) datasets. Our new proxy synthesis ($n = 322$) contains 133 MAP estimates (41%) from Carmichael et al. (2016), 106 data points (33%) from other published sources, and 83 new data points (26%) (**Figure 1; Table S1; Supplementary Data**). The new

data in the compilation helps to improve geographical coverage in previously data-poor regions, including central west coast and eastern Africa (e.g., Eisawi and Schrank, 2008; Adeonipekun et al., 2012; Cantrill et al., 2013) (also recently presented in Williams et al., 2022); the coal and lignite bearing deposits of northeastern India and southern Pakistan (Frederiksen, 1994; Tripathi et al., 2000; Verma et al., 2019); the Tibetan plateau and sedimentary basins of southern China (e.g., Aleksandrova et al., 2015; Su et al., 2020; Xie et al., 2020); and the South American (e.g., Quattrocchio and Volkheimer, 2000; Pardo-Trujillo et al., 2003; Jaramillo et al., 2007) and North American continent and Caribbean islands (e.g., Graham et al., 2000; Jarzen and Klug, 2010; Smith et al., 2020) (**Figure 1; Supplementary Data**). Most of these use the NLR approach based on palynological datasets, as plant macrofossils from the late Paleocene – early Eocene low latitudes are more rarely preserved, although some exceptions are known (Wing et al., 2009; Shukla et al., 2014; Herman et al., 2017). We also incorporate data from the mid and high latitudes, *e.g.*, southern South America, North America, Australia and New Zealand, and high Siberia (**Supplementary Data**). For regions with exceptionally poor data coverage (e.g., tropical and subtropical latitudes, Antarctica), we also compile and generate MAP estimates from the early middle Eocene (47.8 to ~45 Ma; first half of the Lutetian). Published CLAMP and NLR data were re-analysed following recent recommendations, so that there is no bias as a result of discrepant methodology. Specifically, 1) CLAMP-scored fossil leaf assemblages were re-analysed using up-to-date geographically appropriate calibration datasets (Kennedy et al., 2014; Yang et al., 2015; Reichgelt et al., 2019), 2) for both CLAMP and NLR reconstructions, gridded climate datasets from the R package *dismo* were employed (Hijmans et al., 2020), and 3) NLR analysis was performed using consistently filtered modern distribution datasets to avoid regional overrepresentation (e.g. West et al., 2020). Modern site coordinates and age constraints were extracted from the original publications.

Data-model comparison framework

To compare proxy and model data, we employ a data comparison similar to that used for the Miocene MioMIP ensemble (Burls et al., 2021). This approach requires inclusion of uncertainty for both the proxy and model MAP estimates. To account for site location uncertainty, we determine site co-ordinates for the age range of our proxy data compilation above, *i.e.*, from 59 Ma (late Paleocene) to 45 Ma (early middle Eocene) using the Müller et al. (2016) Gplates continental polygons in combination with the hotspot-based rotation frame of Matthews et al. (2016) (*i.e.*, analogous to the DeepMIP simulations; Lunt et al., 2020). For the model simulations, MAP values are taken from the grid cells that fall within the proxy location uncertainty. The model MAP uncertainty is subsequently defined as the range between minimum and maximum MAP within these model grid cells. For proxy estimates, we use the proxy error and error type as reported in the original study. Typically, this is a minimum–maximum range or confidence interval (e.g., 95%) for NLR approaches (e.g., Willard et al., 2019;

West et al., 2020), and standard error (SE) or standard deviation (SD) derived from calibration dataset residuals for leaf physiognomy methods (e.g., Teodoridis et al., 2011). For our newly generated values, uncertainties are reported as 95% confidence interval for NLR and ± 1 SD for CLAMP. The subsequent overlap between the model and proxy uncertainty range is assessed following the MioMIP methodology (Burls et al., 2021). Any overlap between the proxy and model uncertainty ranges is defined as “no bias” (Figure S1 in Burls et al., 2021).

Results and Discussion

DeepMIP models reproduce pre-industrial global precipitation patterns

Each model included in the DeepMIP suite is able to reproduce the main features of pre-industrial global precipitation patterns (**Figure 2**, **Figure S1**). This implies the DeepMIP models can be used to assess the simulated hydrological response in past warm climates (see below). However, some common model precipitation biases are apparent. For example, all simulations exhibit a double-intertropical convergence zone (ITCZ) in MAP, simulating excess precipitation south of the equator. This is expected and the double ICTZ remains a consistent error in both the previous (e.g., CMIP3, CMIP5) and latest (CMIP6) generation of climate models (Tian & Dong 2020). There is also a lack of simulated precipitation in the west central Pacific (**Figure 2c**). However, the shape of the South Pacific convergence zone (SPCZ) is improved in the multi-model mean (MMM) compared to the previous EoMIP generation model simulations (Carmichael et al., 2016).

Influence of non-CO₂ boundary conditions on the early Eocene hydrological cycle

Non-CO₂ boundary conditions (i.e., paleogeography, vegetation, aerosols) can exert an influence on global and regional MAP and $P-E$ values. The previous EoMIP ensemble found a minor role for non-CO₂ boundary conditions on global MAP (+0.1 mm/day; Carmichael et al., 2016). However, this was only performed for a single model simulation (HadCM3L). To fully isolate the influence of non-CO₂ boundary conditions on the early Eocene hydrological cycle, we compared early Eocene 1x CO₂ simulations and pre-industrial 1x CO₂ simulations.

At a global scale, the early Eocene 1x CO₂ simulations are characterised by higher MAP values relative to pre-industrial (> 0.1 to 0.4 mm/day; 1x CO₂ symbols in **Figure 3**). This is because the early Eocene 1x CO₂ simulations have higher global mean surface temperatures ($\sim 3-5^\circ\text{C}$) relative to the preindustrial 1x CO₂ control simulations (see also Lunt et al., 2021) (**Figure S2**). This leads to enhanced surface evaporation which is balanced by precipitation globally

(Held and Soden, 2006; Siler et al., 2019). However, this effect is relatively minor compared to changes in global MAP that occur when CO₂ levels are elevated (*e.g.* >1.4 mm/day at 9x CO₂; **Figure 3**; see Section 3.3).

At a regional scale, the early Eocene 1x CO₂ simulations are characterised by higher MAP estimates in the tropics (0-15° N/S), mid-latitudes (30-60 °N/S), and high-latitude (>60 °N/S) (typically +0.1 to +0.4 mm/day, but up to +0.6 mm/day in the high-latitudes, **Figure 4** and **5**; **Figure S3**) relative to pre-industrial. The tropics (0-15° N/S), mid-latitudes (30-60 °N/S), and high-latitude (>60 °N/S) are also characterised by positive $P-E$ values (typically +0.1 to 0.2 mm/day, but up to +0.4 mm/day in the high-latitudes (**Figure 4** and **6**; **Figure S4** and **S5**) relative to pre-industrial. In the tropics (0-15° N/S) are also characterised by an eastward shift and expansion in deep tropical convection, and hence the Walker Circulation, over the Pacific Ocean (**Figure 4**). The subtropical (15-30 °N/S) early Eocene 1x CO₂ simulations are characterised by negative $P-E$ values (-0.2 to -0.8 mm/day; **Figure 6**; **Figure S4** and **S5**), but the associated MAP estimates span a wide range and can be higher (*i.e.*, CESM, GFDL, MIROC; 0.1 to 0.6 mm/day) or lower (*i.e.*, COSMOS, HadCM3L, HadCM3LB; -0.1 to -0.2 mm/day) relative to pre-industrial (**Figure 5**; **Figure S3**). To diagnose the cause of these differences, we use moisture budget diagnostics to decompose changes in $P-E$ (see discussion below).

Global and regional variability in the early Eocene hydrological cycle

The DeepMIP simulations span a wide range of CO₂ concentrations (x1 to x9 PI CO₂) and global mean surface temperatures (GMST; ~17 to 35°C) and can thus provide insights into the global- and regional-scale hydrological response to CO₂-induced warming. Across the DeepMIP ensemble, higher GMST estimates are associated with higher global MAP estimates as warming leads to enhanced surface evaporation (**Figure 3**). Similar to previous studies (*e.g.* Held and Soden 2006; Siler et al., 2019) the best linear fit across the entire DeepMIP ensemble is a 2.4% increase in global MAP per degree of warming.

There are also regional variations in MAP that differ in their relationship with GMST (**Figure 5**). In the tropics (0–15° N/S), the mid-latitudes (30–60 °N/S) and the high-latitudes (>60 °N/S), higher GMST estimates are associated with higher MAP estimates, with the greatest sensitivity to GMST in the high latitudes (9.1% increase in precipitation per °C warming; **Figure 5d**). This is a consistent feature across the DeepMIP model ensemble. In the subtropics (15–30 °N/S) however, the relationship between GMST and MAP differs between the DeepMIP model simulations. For this latitudinal band there is a wide range in MAP estimates: HadCM3, MIROC and COSMOS simulate lower MAP values relative to pre-industrial, whereas CESM and GFDL simulate higher MAP values relative to pre-industrial (**Figure 5b**). Moisture budget diagnostics (see below) suggest that a weaker latitudinal temperature gradient is the cause of higher MAP values in both CESM and GFDL.

The DeepMIP models also exhibit different regional $P-E$ responses for a given global mean temperature change. In the tropics ($0-15^\circ$ N/S) and the high-latitudes ($>60^\circ$ N/S), higher GMST estimates are associated with more positive $P-E$ values and overall wetter conditions (**Figure 6**). In the subtropics ($15-30^\circ$ N/S), higher GMST estimates are associated with more negative $P-E$ value and overall drier conditions (**Figure 6b**). This indicates that the early Eocene largely conforms to the ‘wet-gets-wetter, dry-gets-drier’ hypothesis within the DeepMIP simulations. Lastly, there is a weak relationship between GMST and $P-E$ values in the mid-latitudes ($30-60^\circ$ N/S; **Figure 6c**). As the mid-latitude band encompasses both positive and negative $P-E$ values compared to pre-industrial (ca. -2 to $+2$ mm/day; **Figure 4**), the lack of relationship between CO_2 and temperature in this zonally-averaged view is perhaps unsurprising.

To diagnose the cause of $P-E$ changes within the DeepMIP ensemble, we conduct a moisture budget analysis, focusing in particular on the zonal mean component (**Figure 7**). This approach relies on the fact that climatological changes in $P-E$, calculated over a long enough timescale that fluctuations in the column integrated moisture content are negligible (in our case the last 100 years of each DeepMIP simulation), are balanced by the column-integrated convergence of moisture in the overlying atmosphere, as follows:

$$P - E = -\nabla \bullet \frac{1}{g} \int_{p_t}^{p_s} \mathbf{v} q \, dp$$

where g is the acceleration due to gravity (ms^{-2}), q the atmospheric specific humidity (kg/kg), and \mathbf{v} the horizontal wind vector (ms^{-1}) integrated across (decreasing) pressure (p , Pa) levels from the surface (p_s) to the top of the troposphere (tropopause; p_t) (**Figure 7a-b**). This moisture convergence can be further decomposed into its time mean ($\bar{v} \bar{q}$) and eddy ($\overline{v' q'}$) components (**Figure 7c-d**; **Figure S6**). Generally speaking, the time mean component is the dominant component in the tropics, where the time mean moisture transport typically dominates over the eddy component (**Figure 7c-7d**). Changes in net $P-E$ values ($\delta(P-E)$) due to the time mean component can be further decomposed into: i) changes in humidity assuming constant preindustrial circulation ($\bar{v}_{\text{cnt}} \delta \bar{q}$, the thermodynamic component of changes in the time mean moisture divergence), ii) changes in circulation assuming constant preindustrial humidity ($\delta \bar{v} \bar{q}_{\text{cnt}}$, the dynamic component of changes in the time mean moisture divergence), and iii) a perturbation term representing the coupling of changes in humidity and changes in circulation ($\delta \bar{v} \delta \bar{q}$) (**Figures 7e-f**; **Figure S7**):

$$\delta(P-E) = -\nabla \bullet \frac{1}{g} \int_{p_t}^{p_s} v_{\text{cnt}} q \, dp - \nabla \bullet \frac{1}{g} \int_{p_t}^{p_s} \delta v v q_{\text{cnt}} \, dp - \nabla \bullet \frac{1}{g} \int_{p_t}^{p_s} \delta v \, q \, dp$$

where δ represents the change in each variable between the study interval (i.e., the early Eocene) and the pre-industrial climate. With increasing tempera-

tures, atmospheric humidity (q) is predicted to increase following the Clausius-Clapeyron relation. Assuming that circulation (v) remains identical to pre-industrial ($\delta v = 0$), the dynamic term will be zero and the thermodynamic term will result in the tropics and high-latitudes becoming wetter (i.e. the moisture convergence into these regions in the control climate is enhanced) and the subtropics becoming drier (i.e., the moisture divergence from this region in the control climate is enhanced). Circulation changes are often considered secondary to changes in atmospheric humidity. However, it has been demonstrated the former may be important under certain climate scenarios (e.g., weak latitudinal temperature gradients) and may even compensate for changes in atmospheric humidity (Burls & Fedorov 2017). In a scenario where circulation (v) – specifically a decrease in Hadley cell strength – dominates over an increase in humidity (q), the subtropics will be characterised by reduced (rather than enhanced) moisture divergence and wetter (rather than drier) conditions.

Focusing on the subtropics in the DeepMIP simulations, higher GMST values result in an increase in atmospheric humidity and enhanced subtropical moisture divergence. This leads to a corresponding decrease in $P-E$ (up to > -1.5 mm/day; **Figure 8a**) and is consistent with a ‘wet-gets-wetter, dry-gets-drier’ scenario in warmer climates. However, this is partially compensated by a reduction in LTGs, here taken as the difference between 15°S – 15°N and 30 – 60°N/S . Reduced LTGs lead to a reduction in the strength of subtropical moisture circulation (v) and a relative increase in subtropical $P-E$ (**Figure 8b**). This dynamical effect is stronger in model simulations with weaker latitudinal temperature gradients (i.e., CESM and GFDL model simulations) and weaker in models with stronger latitudinal temperature gradients (e.g., HadCM3L). This explains why DeepMIP models with the lowest LTGs (e.g. CESM and GFDL) are characterised by higher MAP estimates relative to pre-industrial. Intriguingly, those models with reduced LTGs most closely reproduce temperature gradients (and GMST estimates) as reconstructed by proxies (Figure 1 in Lunt et al., 2021). This implies that the early Eocene was likely characterised by a reduction in the strength of subtropical moisture circulation. However, all DeepMIP models, including CESM and GFDL, show that this reduction in subtropical moisture circulation (**Figure 8d**) was not sufficient to compensate fully for changes in atmospheric humidity (**Figure 8c**). As such, the subtropics are characterised by overall drier conditions in terms of $P-E$ (**Figure 8a**).

Extrapolating from this, if early Eocene LTGs were weaker than suggested by these models (Lunt et al., 2021), changes in strength of subtropical moisture circulation may outcompete changes in enhanced moisture divergence, leading to overall wetter subtropics (see Burls & Federov, 2017). Although proxy-model bias is decreasing for certain models, overall, early Eocene proxy compilations suggest weaker global pole-to-equator LTGs (~ 14 – 22°C ; Gaskell et al., 2022; Evans et al., 2018; Cramwinckel et al., 2018) than predicted in the DeepMIP model ensemble (~ 18 to 25°C ; Figure 1b in Lunt et al., 2021). However, proxy-derived LTG estimates remain associated with large uncertainties due to the use of different input datasets and/or the analysis of different time intervals (*cf.*

GMST estimates; Inglis et al., 2020). Taken together, this highlights the important role of the meridional temperature gradient when interpreting subtropical rainfall patterns.

Proxy-based precipitation estimates during the early Eocene

Our proxy synthesis indicates that high-latitude regions were characterised by high MAP estimates, consistent with previous results from the northern (Eberle and Greenwood, 2012; West et al., 2015; Suan et al., 2017; Salpin et al., 2019; West et al., 2020) and southern high-latitudes (Poole et al., 2005; Pross et al., 2012) (**Figure 9**). This is consistent with evidence for low-salinity sea surface conditions in the high northern latitudes near the termination of the EECO (~49 Ma) (i.e., the Azolla interval) (Brinkhuis et al., 2006; Barke et al., 2012). Proxy estimates from more transient warming events (e.g., the PETM and Eocene Thermal Maximum 2; ETM2) provide additional support for high MAP in the Arctic (Pagani et al., 2006; Willard et al., 2019), the North Sea Basin (Kender et al., 2012; Garel et al., 2013; Collinson et al., 2003), and the southwest Pacific (Sluijs et al., 2011; Pancost et al., 2013). We note that in our compilation, early Eocene-aged CLAMP-derived MAP estimates from North America are much higher than most NLR estimates. CLAMP estimates are based on locally derived floral assemblages, whereas NLR estimates can reflect both locally derived floral elements but also floral elements transported over long distance (e.g. wind- or water-dispersed pollen). As a consequence, CLAMP estimates may reflect a bias towards wetter environments, whereas NLR estimates may be biased towards drier (upland) environments. The set of MAP estimates from Antarctica based on wood physiognomy are also far higher than the other proxies (Poole et al., 2005). Due to the lack of wood physiognomic MAP estimates from other regions, it is unclear whether these values are representative of the Antarctic continent.

Early Eocene tropical and subtropical MAP estimates are also relatively high (> 2 to 4 mm/day). Although proxy-derived subtropical MAP values imply wetter conditions during the early Eocene (see above), these estimates are biased towards regions with well-preserved floral assemblages and, by extension, relatively wet regions. Subsequently, arid and semi-arid environments are likely under sampled in our synthesis. Indeed, evidence from other climate intervals (e.g., the PETM) suggests drier subtropics, with evidence for enhanced evapotranspiration in Tanzania during the onset of the PETM (Handley et al., 2012), drying in the continental interior (e.g., Bighorn Basin) during the body of the PETM (Smith et al., 2007; Kraus and Riggins, 2007; Kraus et al., 2013), and increased subtropical salinity in the central Pacific during ETM2 (Harper et al., 2017). Moving forward, we suggest that alternative proxies, for example clumped isotope- ^{18}O analysis of pedogenic siderites (van Dijk et al., 2020), could help to reconstruct hydrological change in arid and semi-arid environments where plant macrofossils are unlikely to be preserved, and the availability

of plant-based terrestrial proxy data will therefore be limited or absent.

Terrestrial precipitation data-model comparison

To explore whether the DeepMIP models realistically reproduce regional MAP patterns during the early Eocene, we employ a data-model comparison (following Burls et al., 2021) using our new and published botanical-based MAP estimates. A previous site-by-site data-model comparison (Carmichael et al., 2016) suggested that the EoMIP models were able to reproduce key features of the hydrological cycle in the mid-latitudes (e.g., western US interior, central Europe), but modelled MAP estimates were typically lower than those from proxies in the high-latitudes (e.g., East Antarctica, SE Australia, Axel Heiberg). In the new DeepMIP compilation, we find that the multi-model mean (MMM) is able to replicate MAP estimates in various regional bands (i.e., the tropics, subtropics and southern high latitudes) within error (**Figure 10**). However, the MMM underestimates proxy-derived MAP in the high northern latitudes, especially at lower CO₂ levels (**Figure 10**). We attribute this mismatch to the lack of polar amplification in certain models, especially at lower CO₂ levels (e.g., HadCM3, COSMOS) (Lunt et al., 2021). The mid-latitudes are likewise associated with a large data-model mismatch. Here, the MMM either underestimates MAP (e.g., western South America and Tibet) or overestimates MAP (e.g., western North America; **Figure 10**). As these mismatches lie close to major mountain ranges (e.g., Rockies, proto-Tibetan Plateau, Andes), it is possible that mismatches are largely due to topographic effects. For a given model, the data-model mismatch is lowest for CESM and GFDL, i.e., the models with higher GMST estimates and lower LTGs (Lunt et al., 2021) (**Figure 11**; **Figure S8**). Our results indicate that the models with higher GMST estimates and weaker LTGs are able to better simulate the global and regional scale hydrological cycle. Overall, our integrated data-model approach suggests that the early Eocene was characterised by a thermodynamically-dominated hydrological response to warming within the mid and high latitudes, with increased CO₂ forcing improving the model-proxy fit by increasing precipitation (**Figure 11c-d**; **Figure S8**). Overall, the DeepMIP models show a slight overshoot in precipitation in the tropics (**Figure 11a**; **Figure S8**). Lastly, in the subtropical latitudes, dynamical changes in large-scale circulation in response to weaker surface temperature gradients could have supported regional wetting, as seen to some extent in the GFDL and CESM models (**Figure 11b**; **Figure S8**).

Conclusions

Here we use the DeepMIP model simulations to reconstruct global- and regional-scale rainfall patterns during the early Eocene (~56–48 million years ago), with an emphasis on the subtropical hydrological cycle. At higher temperatures, model simulations indicate that low- (0–15° N/S) and high-latitudes (>60° N/S) are characterised by positive $P-E$ values (wetter conditions), whereas the sub-

tropics (15-30° N/S) are characterised by negative $P-E$ values (drier conditions). The DeepMIP models can (partly) replicate proxy-derived MAP estimates in various regional bands (i.e., the tropics, subtropics and southern high latitudes) within error, especially at high CO₂ and in models with weaker latitudinal temperature gradients. This indicates that the early Eocene was overall characterised by a thermodynamically-dominated ‘wet-gets-wetter, dry-gets-drier’ response in the mid and high latitudes. However, there is large inter-model variability in subtropical mean annual precipitation (MAP) due to the competing influence of humidity (i.e., thermodynamic changes) and atmospheric moisture circulation (i.e., dynamic changes) in this region. We show that models with weaker latitudinal temperature gradients are characterised by a reduction in subtropical moisture circulation, leading to an overall increase in subtropical MAP. Crucially, these models agree more closely with proxy-derived precipitation estimates and imply weaker subtropical moisture circulation in the early Eocene. However, changes in subtropical moisture circulation were not sufficient to induce subtropical wetting. Taken together, our study highlights the importance of the meridional temperature gradient when studying past (and future) subtropical rainfall patterns.

Open Research

The proxy data used in the study are available at Pangaea (DOI to follow) and associated with a CC-BY 4.0 license.

Acknowledgments

G.N.I and M.C. were supported by a Royal Society Dorothy Hodgkin Fellowship (DHF\R1\191178). N.B. was supported by the National Science Foundation, via award AGS-1844380. D.G was supported by the Natural Sciences and Engineering Research Council of Canada (NSERC) through Discovery Grants (DG 311934 and 2016-04337). C.K.W acknowledges funding from a private donor to the Northern Climates Postdoctoral Fellowship at the University of Alberta. D.K.H acknowledges support from Australian Research Council grant DE22010079 and the Australian Centre for Excellence in Antarctic Science, project number SR200100008. R.F is supported by NSF-2114204. A.dB was supported by Swedish Research Council project 2020-04791. The GFDL simulations were performed by resources provided by the Swedish National Infrastructure for Computing (SNIC) at the National Supercomputer Centre (NSC), partially funded by the Swedish Research Council through grant agreement no. 2018-05973. W.L.C and A.A.O acknowledge funding from JSPS KAKENHI (Grant no. 17H06104) and MEXT KAKENHI (Grant no. 17H06323).

Conflict of Interest

The authors declare no conflicts of interest relevant to this study.

Reference list

Adeonipekun, P. A., Ehinola, O. A., Toluhi, Yussuph, I. A., Toluhi, A., and Oyelami, A.: Bio-Sequence Stratigraphy of Shagamu Quarry Outcrop, Benin Basin, Southwestern Nigeria, 2012. Aleksandrova, G. N., Kodrul, T. M., and Jin, J. H.: Palynological and paleobotanical investigations of Paleogene sections in the Maoming basin, South China, *Stratigr. Geol. Correl.*, 23, 300–325, <https://doi.org/10.1134/S0869593815030028>, 2015. Anagnostou, E., John, E. H., Babila, T. L., Sexton, P. F., Ridgwell, A., Lunt, D. J., Pearson, P. N., Chalk, T. B., Pancost, R. D., and Foster, G. L.: Proxy evidence for state-dependence of climate sensitivity in the Eocene greenhouse, *Nat. Commun.*, 11, 4436, <https://doi.org/10.1038/s41467-020-17887-x>, 2020. Barke, J., van der Burgh, J., van Konijnenburg-van Cittert, J. H. A., Collinson, M. E., Pearce, M. A., Bujak, J., Heilmann-Clausen, C., Speelman, E. N., van Kempen, M. M. L., Reichart, G.-J., Lotter, A. F., and Brinkhuis, H.: Coeval Eocene blooms of the freshwater fern *Azolla* in and around Arctic and Nordic seas, *Palaeogeogr. Palaeoclimatol. Palaeoecol.*, 337–338, 108–119, <https://doi.org/10.1016/j.palaeo.2012.04.002>, 2012. Brinkhuis, H., Schouten, S., Collinson, M. E., Sluijs, A., Damsté, J. S. S., Dickens, G. R., Huber, M., Cronin, T. M., Onodera, J., Takahashi, K., Bujak, J. P., Stein, R., van der Burgh, J., Eldrett, J. S., Harding, I. C., Lotter, A. F., Sangiorgi, F., Cittert, H. van K., de Leeuw, J. W., Matthiessen, J., Backman, J., Moran, K., and the Expedition 302 Scientists: Episodic fresh surface waters in the Eocene Arctic Ocean, *Nature*, 441, 606–609, <https://doi.org/10.1038/nature04692>, 2006. Burls, N. J., Bradshaw, C. D., Boer, A. M. D., Herold, N., Huber, M., Pound, M., Donnadieu, Y., Farnsworth, A., Frigola, A., Gasson, E., Heydt, A. S. von der, Hutchinson, D. K., Knorr, G., Lawrence, K. T., Lear, C. H., Li, X., Lohmann, G., Lunt, D. J., Marzocchi, A., Prange, M., Riihimaki, C. A., Sarr, A.-C., Siler, N., and Zhang, Z.: Simulating Miocene Warmth: Insights From an Opportunistic Multi-Model Ensemble (MioMIP1), *Paleoceanogr. Paleoclimatology*, 36, e2020PA004054, <https://doi.org/10.1029/2020PA004054>, 2021. Cantrill, D. J., Bamford, M. K., Wagstaff, B. E., and Sauquet, H.: Early Eocene fossil plants from the Mwadui kimberlite pipe, Tanzania, *Rev. Palaeobot. Palynol.*, 196, 19–35, <https://doi.org/10.1016/j.revpalbo.2013.04.002>, 2013. Carmichael, M. J., Lunt, D. J., Huber, M., Heinemann, M., Kiehl, J., LeGrande, A., Loptson, C. A., Roberts, C. D., Sagoo, N., Shields, C., Valdes, P. J., Winguth, A., Winguth, C., and Pancost, R. D.: A model–model and data–model comparison for the early Eocene hydrological cycle, *Clim Past*, 12, 455–481, <https://doi.org/10.5194/cp-12-455-2016>, 2016. Carmichael, M. J., Inglis, G. N., Badger, M. P. S., Naafs, B. D. A., Behrooz, L., Rimmelzwaal, S., Monteiro, F. M., Rohrssen, M., Farnsworth, A., Buss, H. L., Dickson, A. J., Valdes, P. J., Lunt, D. J., and Pancost, R. D.: Hydrological and associated biogeochemical consequences of rapid global warming during the Paleocene-Eocene Thermal Maximum, *Glob. Planet. Change*, 157, 114–138, <https://doi.org/10.1016/j.gloplacha.2017.07.014>, 2017. Carrapa, B., Clementz, M., and Feng, R.: Ecological and hydroclimate responses to strengthening of

the Hadley circulation in South America during the Late Miocene cooling, *Proc. Natl. Acad. Sci.*, 116, 9747–9752, <https://doi.org/10.1073/pnas.1810721116>, 2019.

Collinson, M. E., Hooker, J. J., and Groecke, D. R.: Cobham lignite bed and penecontemporaneous macrofloras of southern England: A record of vegetation and fire across the Paleocene-Eocene Thermal Maximum, <https://doi.org/10.1130/0-8137-2369-8.333>, 2003.

Cramwinckel, M. J., Huber, M., Kocken, I. J., Agnini, C., Bijl, P. K., Bohaty, S. M., Frieling, J., Goldner, A., Hilgen, F. J., Kip, E. L., Peterse, F., Ploeg, R. van der, Röhl, U., Schouten, S., and Sluijs, A.: Synchronous tropical and polar temperature evolution in the Eocene, *Nature*, 559, 382–386, <https://doi.org/10.1038/s41586-018-0272-2>, 2018.

van Dijk, J., Fernandez, A., Bernasconi, S. M., Caves Rügenstein, J. K., Passey, S. R., and White, T.: Spatial pattern of super-greenhouse warmth controlled by elevated specific humidity, *Nat. Geosci.*, 13, 739–744, <https://doi.org/10.1038/s41561-020-00648-2>, 2020.

Eberle, J. J. and Greenwood, D. R.: Life at the top of the greenhouse Eocene world—A review of the Eocene flora and vertebrate fauna from Canada’s High Arctic, *Geol. Soc. Am. Bull.*, 124, 3–23, <https://doi.org/10.1130/B30571.1>, 2012.

Eisawi, A. and Schrank, E.: Upper Cretaceous to Neogene palynology of the Melut Basin, Southeast Sudan, *Palynology*, 32, 101–129, <https://doi.org/10.1080/01916122.2008.9989653>, 2008.

Evans, D., Sagoo, N., Renema, W., Cotton, L. J., Müller, W., Todd, J. A., Saraswati, P. K., Stassen, P., Ziegler, M., Pearson, P. N., Valdes, P. J., and Affek, H. P.: Eocene greenhouse climate revealed by coupled clumped isotope-Mg/Ca thermometry, *Proc. Natl. Acad. Sci.*, 201714744, <https://doi.org/10.1073/pnas.1714744115>, 2018.

Eyring, V., Bony, S., Meehl, G. A., Senior, C. A., Stevens, B., Stouffer, R. J., and Taylor, K. E.: Overview of the Coupled Model Intercomparison Project Phase 6 (CMIP6) experimental design and organization, *Geosci. Model Dev.*, 9, 1937–1958, <https://doi.org/10.5194/gmd-9-1937-2016>, 2016.

Fauquette, S., Guiot, J., and Suc, J.-P.: A method for climatic reconstruction of the Mediterranean Pliocene using pollen data, *Palaeogeogr. Palaeoclimatol. Palaeoecol.*, 144, 183–201, [https://doi.org/10.1016/S0031-0182\(98\)00083-2](https://doi.org/10.1016/S0031-0182(98)00083-2), 1998.

Frederiksen, N. O.: Middle and late paleocene angiosperm pollen from Pakistan, *Palynology*, 18, 91–137, <https://doi.org/10.1080/01916122.1994.9989442>, 1994.

Garel, S., Schnyder, J., Jacob, J., Dupuis, C., Boussafir, M., Le Milbeau, C., Storme, J.-Y., Iakovleva, A. I., Yans, J., Baudin, F., Fléhoc, C., and Quesnel, F.: Paleohydrological and paleoenvironmental changes recorded in terrestrial sediments of the Paleocene–Eocene boundary (Normandy, France), *Palaeogeogr. Palaeoclimatol. Palaeoecol.*, 376, 184–199, <https://doi.org/10.1016/j.palaeo.2013.02.035>, 2013.

Gaskell, D. E., Huber, M., O’Brien, C. L., Inglis, G. N., Acosta, R. P., Poulsen, C. J., and Hull, P. M.: The latitudinal temperature gradient and its climate dependence as inferred from foraminiferal $\delta^{18}O$ over the past 95 million years, *Proc. Natl. Acad. Sci.*, 119, e2111332119, <https://doi.org/10.1073/pnas.2111332119>, 2022.

Givnish, T. J.: Leaf and Canopy Adaptations in Tropical Forests, in: *Physiological ecology of plants of the wet tropics*, vol. 12, edited by: Medina, E., Mooney, H. A., and Vázquez-Yanes, C., Springer Netherlands, Dordrecht, 51–84,

https://doi.org/10.1007/978-94-009-7299-5_6, 1984. Graham, A., Cozadd, D., Areces-Mallea, A., and Frederiksen, N. O.: Studies in Neotropical paleobotany. XIV. A palynoflora from the Middle Eocene Saramaguacán Formation of Cuba, *Am. J. Bot.*, 87, 1526–1539, <https://doi.org/10.2307/2656879>, 2000. Greenwood, D. R.: Fossil angiosperm leaves and climate: from Wolfe and Dilcher to Burnham and Wilf, *Cour. Forschungsinstitut Senckenberg*, 258, 95–108, 2007. Greenwood, D. R., Moss, P. T., Rowett, A. I., Vadala, A. J., and Keefe, R. L.: Plant communities and climate change in southeastern Australia during the early Paleogene, in: Causes and consequences of globally warm climates in the early Paleogene, edited by: Wing, S. L., Gingerich, P. D., Schmitz, B., and Thomas, E., Geological Society of America, 365–380, 2003. Hailemichael, M., Aronson, J. L., Savin, S., Tevesz, M. J. S., and Carter, J. G.: 18O in mollusk shells from Pliocene Lake Hadar and modern Ethiopian lakes: implications for history of the Ethiopian monsoon, *Palaeogeogr. Palaeoclimatol. Palaeoecol.*, 186, 81–99, [https://doi.org/10.1016/S0031-0182\(02\)00445-5](https://doi.org/10.1016/S0031-0182(02)00445-5), 2002. Handley, L., O’Halloran, A., Pearson, P. N., Hawkins, E., Nicholas, C. J., Schouten, S., McMillan, I. K., and Pancost, R. D.: Changes in the hydrological cycle in tropical East Africa during the Paleocene–Eocene Thermal Maximum, *Palaeogeogr. Palaeoclimatol. Palaeoecol.*, 329–330, 10–21, <https://doi.org/10.1016/j.palaeo.2012.02.002>, 2012. Harper, D. T., Zeebe, R., Hönisch, B., Schrader, C. D., Lourens, L. J., and Zachos, J. C.: Subtropical sea-surface warming and increased salinity during Eocene Thermal Maximum 2, *Geology*, 46, 187–190, <https://doi.org/10.1130/G39658.1>, 2017. Held, I. M. and Soden, B. J.: Robust Responses of the Hydrological Cycle to Global Warming, *J. Clim.*, 19, 5686–5699, <https://doi.org/10.1175/JCLI3990.1>, 2006. Herman, A. B., Spicer, R. A., Aleksandrova, G. N., Yang, J., Kodrul, T. M., Maslova, N. P., Spicer, T. E. V., Chen, G., and Jin, J.-H.: Eocene–early Oligocene climate and vegetation change in southern China: Evidence from the Maoming Basin, *Palaeogeogr. Palaeoclimatol. Palaeoecol.*, 479, 126–137, <https://doi.org/10.1016/j.palaeo.2017.04.023>, 2017. Herold, N., Buzan, J., Seton, M., Goldner, A., Green, J. A. M., Müller, R. D., Markwick, P., and Huber, M.: A suite of early Eocene (~ 55 Ma) climate model boundary conditions, *Geosci Model Dev*, 7, 2077–2090, <https://doi.org/10.5194/gmd-7-2077-2014>, 2014. Hijmans, R. J., Phillips, S., Leathwick, J., and Elith, J.: dismo: Species Distribution Modeling, 2020. Hoegh-Guldberg, O., Jacob, D., Taylor, M., Bindi, M., Brown, S., Camilloni, I., Diedhiou, A., Djalante, R., Ebi, K. L., Engelbrecht, F., Guiot, J., Hijioka, Y., Mehrotra, S., Payne, A., Seneviratne, S. I., Thomas, A., Warren, R., and Zhou, G.: Impacts of 1.5°C Global Warming on Natural and Human Systems, in: Global Warming of 1.5°C. An IPCC Special Report on the impacts of global warming of 1.5°C above pre-industrial levels and related global greenhouse gas emission pathways, in the context of strengthening the global response to the threat of climate change, sustainable development, and efforts to eradicate poverty, edited by: Masson-Delmotte, V., Zhai, P., Pörtner, H.-O., Roberts, D., Skea, J., Shukla, P. R., Pirani, A., Moufouma-Okia, W., Péan, C., Pidcock, R., Connors, S., Matthews, J. B. R., Chen, Y., Zhou, X., Gomis, M. I., Lonnoy, E., Maycock, T., Tignor, M., and Waterfield, T., In

press, 2018. Inglis, G. N., Bragg, F., Burls, N. J., Cramwinckel, M. J., Evans, D., Foster, G. L., Huber, M., Lunt, D. J., Siler, N., Steinig, S., Tierney, J. E., Wilkinson, R., Anagnostou, E., de Boer, A. M., Dunkley Jones, T., Edgar, K. M., Hollis, C. J., Hutchinson, D. K., and Pancost, R. D.: Global mean surface temperature and climate sensitivity of the early Eocene Climatic Optimum (EECO), Paleocene–Eocene Thermal Maximum (PETM), and latest Paleocene, *Clim. Past*, 16, 1953–1968, <https://doi.org/10.5194/cp-16-1953-2020>, 2020. Jaramillo, C. A., Bayona, G., Pardo-Trujillo, A., Rueda, M., Torres, V., Harrington, G. J., and Mora, G.: THE PALYNOLOGY OF THE CERREJÓN FORMATION (UPPER PALEOCENE) OF NORTHERN COLOMBIA, *Palynology*, 31, 153–189, <https://doi.org/10.2113/gspalynol.31.1.153>, 2007. Jarzen, D. M. and Klug, C.: A preliminary investigation of a lower to middle Eocene palynoflora from Pine Island, Florida, USA, *Palynology*, 34, 164–179, <https://doi.org/10.1080/01916121003737421>, 2010. Kender, S., Stephenson, M. H., Riding, J. B., Leng, M. J., Knox, R. W. O., Peck, V. L., Kendrick, C. P., Ellis, M. A., Vane, C. H., and Jamieson, R.: Marine and terrestrial environmental changes in NW Europe preceding carbon release at the Paleocene–Eocene transition, *Earth Planet. Sci. Lett.*, 353–354, 108–120, <https://doi.org/10.1016/j.epsl.2012.08.011>, 2012. Kennedy, E. M., Arens, N. C., Reichgelt, T., Spicer, R. A., Spicer, T. E. V., Stranks, L., and Yang, J.: Deriving temperature estimates from Southern Hemisphere leaves, *Palaeogeogr. Palaeoclimatol. Palaeoecol.*, 412, 80–90, <https://doi.org/10.1016/j.palaeo.2014.07.015>, 2014. Kraus, M. J. and Riggins, S.: Transient drying during the Paleocene–Eocene Thermal Maximum (PETM): Analysis of paleosols in the bighorn basin, Wyoming, *Palaeogeogr. Palaeoclimatol. Palaeoecol.*, 245, 444–461, <https://doi.org/10.1016/j.palaeo.2006.09.011>, 2007. Kraus, M. J., McInerney, F. A., Wing, S. L., Secord, R., Baczynski, A. A., and Bloch, J. I.: Paleohydrologic response to continental warming during the Paleocene–Eocene Thermal Maximum, Bighorn Basin, Wyoming, *Palaeogeogr. Palaeoclimatol. Palaeoecol.*, 370, 196–208, <https://doi.org/10.1016/j.palaeo.2012.12.008>, 2013. Lunt, D. J., Bragg, F., Chan, W.-L., Hutchinson, D. K., Ladant, J.-B., Morozova, P., Niezgodzki, I., Steinig, S., Zhang, Z., Zhu, J., Abe-Ouchi, A., Anagnostou, E., de Boer, A. M., Coxall, H. K., Donnadieu, Y., Foster, G., Inglis, G. N., Knorr, G., Langebroek, P. M., Lear, C. H., Lohmann, G., Poulsen, C. J., Sepulchre, P., Tierney, J. E., Valdes, P. J., Volodin, E. M., Dunkley Jones, T., Hollis, C. J., Huber, M., and Otto-Bliesner, B. L.: DeepMIP: model intercomparison of early Eocene climatic optimum (EECO) large-scale climate features and comparison with proxy data, *Clim. Past*, 17, 203–227, <https://doi.org/10.5194/cp-17-203-2021>, 2021. Masson-Delmotte, V., Zhai, P., Pirani, A., Connors, S. L., Péan, C., Chen, Y., Goldfarb, L., Gomis, M. I., Matthews, J. B. R., Berger, S., Huang, M., Yelekçi, O., Yu, R., Zhou, B., Lonnoy, E., Maycock, T. K., Waterfield, T., and Leitzell, K.: IPCC, 2021: Climate Change 2021: The Physical Science Basis. Contribution of Working Group I to the Sixth Assessment Report of the Intergovernmental Panel on Climate Change, Cambridge University Press, Cambridge, United Kingdom and New York, NY, USA, 2022. Matthews, K. J., Maloney, K. T., Zahirovic, S., Williams, S. E., Seton, M., and Müller, R. D.:

Global plate boundary evolution and kinematics since the late Paleozoic, *Glob. Planet. Change*, 146, 226–250, <https://doi.org/10.1016/j.gloplacha.2016.10.002>, 2016. Mosbrugger, V. and Utescher, T.: The coexistence approach — a method for quantitative reconstructions of Tertiary terrestrial palaeoclimate data using plant fossils, *Palaeogeogr. Palaeoclimatol. Palaeoecol.*, 134, 61–86, [https://doi.org/10.1016/S0031-0182\(96\)00154-X](https://doi.org/10.1016/S0031-0182(96)00154-X), 1997. Müller, R. D., Seton, M., Zahirovic, S., Williams, S. E., Matthews, K. J., Wright, N. M., Shephard, G. E., Maloney, K. T., Barnett-Moore, N., Hosseinpour, M., Bower, D. J., and Cannon, J.: Ocean Basin Evolution and Global-Scale Plate Reorganization Events Since Pangea Breakup, *Annu. Rev. Earth Planet. Sci.*, 44, 107–138, <https://doi.org/10.1146/annurev-earth-060115-012211>, 2016. Pagni, M., Pedentchouk, N., Huber, M., Shuijs, A., Schouten, S., Brinkhuis, H., Sinninghe Damsté, J. S., Dickens, G. R., Expedition 302 Scientists, Backman, J., Clemens, S., Cronin, T., Eynaud, F., Gattacceca, J., Jakobsson, M., Jordan, R., Kaminski, M., King, J., Koc, N., Martinez, N. C., McInroy, D., Jr, T. C. M., O’Regan, M., Onodera, J., Pälike, H., Rea, B., Rio, D., Sakamoto, T., Smith, D. C., John, K. E. K. S., Suto, I., Suzuki, N., Takahashi, K., Watanabe, M., and Yamamoto, M.: Arctic hydrology during global warming at the Palaeocene/Eocene thermal maximum, *Nature*, 442, 671–675, <https://doi.org/10.1038/nature05043>, 2006. Pancost, R. D., Taylor, K. W. R., Inglis, G. N., Kennedy, E. M., Handley, L., Hollis, C. J., Crouch, E. M., Pross, J., Huber, M., Schouten, S., Pearson, P. N., Morgans, H. E. G., and Raine, J. I.: Early Paleogene evolution of terrestrial climate in the SW Pacific, Southern New Zealand, *Geochem. Geophys. Geosystems*, 14, 5413–5429, <https://doi.org/10.1002/2013GC004935>, 2013. Pardo-Trujillo, A., Jaramillo, C. A., and Oboh-Ikuenobe, F. E.: Paleogene palynostratigraphy of the eastern middle Magdalena Valley, Colombia, *Palynology*, 27, 155–178, <https://doi.org/10.1080/01916122.2003.9989585>, 2003. Peppe, D. J., Royer, D. L., Cariglino, B., Oliver, S. Y., Newman, S., Leight, E., Enikolopov, G., Fernandez-Burgos, M., Herrera, F., Adams, J. M., Correa, E., Curran, E. D., Erickson, J. M., Hinojosa, L. F., Hoganson, J. W., Iglesias, A., Jaramillo, C. A., Johnson, K. R., Jordan, G. J., Kraft, N. J. B., Lovelock, E. C., Lusk, C. H., Niinemets, Ü., Peñuelas, J., Rapson, G., Wing, S. L., and Wright, I. J.: Sensitivity of leaf size and shape to climate: global patterns and paleoclimatic applications, *New Phytol.*, 190, 724–739, <https://doi.org/10.1111/j.1469-8137.2010.03615.x>, 2011. Poole, I. and van Bergen, P. F.: Physiognomic and chemical characters in wood as palaeoclimate proxies, in: *Plants and Climate Change*, edited by: Rozema, J., Aerts, R., and Cornelissen, H., Springer Netherlands, Dordrecht, 175–196, https://doi.org/10.1007/978-1-4020-4443-4_12, 2006. Poole, I., Cantrill, D., and Utescher, T.: A multi-proxy approach to determine Antarctic terrestrial palaeoclimate during the Late Cretaceous and Early Tertiary, *Palaeogeogr. Palaeoclimatol. Palaeoecol.*, 222, 95–121, <https://doi.org/10.1016/j.palaeo.2005.03.011>, 2005. Prasad, V., Utescher, T., Sharma, A., Singh, I. B., Garg, R., Gogoi, B., Srivastava, J., Uddandam, P. R., and Joachimski, M. M.: Low-latitude vegetation and climate dynamics at the Paleocene-Eocene transition – A study based on multiple proxies

from the Jathang section in northeastern India, *Palaeogeogr. Palaeoclimatol. Palaeoecol.*, 497, 139–156, <https://doi.org/10.1016/j.palaeo.2018.02.013>, 2018. Pross, J., Klotz, S., and Mosbrugger, V.: Reconstructing palaeotemperatures for the Early and Middle Pleistocene using the mutual climatic range method based on plant fossils, *Quat. Sci. Rev.*, 19, 1785–1799, [https://doi.org/10.1016/S0277-3791\(00\)00089-5](https://doi.org/10.1016/S0277-3791(00)00089-5), 2000. Pross, J., Contreras, L., Bijl, P. K., Greenwood, D. R., Bohaty, S. M., Schouten, S., Bendle, J. A., Röhl, U., Tauxe, L., Raine, J. I., Huck, C. E., van de Flierdt, T., Jamieson, S. S. R., Stickley, C. E., van de Schootbrugge, B., Escutia, C., Brinkhuis, H., and Scientists, I. O. D. P. E. 318: Persistent near-tropical warmth on the Antarctic continent during the early Eocene epoch, *Nature*, 488, 73–77, <https://doi.org/10.1038/nature11300>, 2012. Quattrocchio, M. E. and Volkheimer, W.: Paleoclimatic Changes during the Paleocene-Lower Eocene in the Salta Group Basin, NW Argentina, in: *Southern Hemisphere Paleo- and Neoclimates: Key Sites, Methods, Data and Models*, edited by: Smolka, P. and Volkheimer, W., Springer, Berlin, Heidelberg, 353–367, https://doi.org/10.1007/978-3-642-59694-0_22, 2000. Reichgelt, T., Kennedy, E. M., Conran, J. G., Lee, W. G., and Lee, D. E.: The presence of moisture deficits in Miocene New Zealand, *Glob. Planet. Change*, 172, 268–277, <https://doi.org/10.1016/j.gloplacha.2018.10.013>, 2019. Salpin, M., Schnyder, J., Baudin, F., Suan, G., Suc, J.-P., Popescu, S.-M., Fauquette, S., Reinhardt, L., Schmitz, M. D., and Labrousse, L.: Evidence for subtropical warmth in the Canadian Arctic (Beaufort-Mackenzie, Northwest Territories, Canada) during the early Eocene, [https://doi.org/10.1130/2018.2541\(27\)](https://doi.org/10.1130/2018.2541(27)), 2019. Schuster, M., Düringer, P., Ghienne, J.-F., Roquin, C., Sepulchre, P., Moussa, A., Lebatard, A.-E., Mackaye, H. T., Likius, A., Vignaud, P., and Brunet, M.: Chad Basin: Paleoenvironments of the Sahara since the Late Miocene, *Comptes Rendus Geosci.*, 341, 603–611, <https://doi.org/10.1016/j.crte.2009.04.001>, 2009. Seager, R., Naik, N., and Vecchi, G. A.: Thermodynamic and Dynamic Mechanisms for Large-Scale Changes in the Hydrological Cycle in Response to Global Warming, *J. Clim.*, 23, 4651–4668, <https://doi.org/10.1175/2010JCLI3655.1>, 2010. Shukla, A., Mehrotra, R. C., Spicer, R. A., Spicer, T. E. V., and Kumar, M.: Cool equatorial terrestrial temperatures and the South Asian monsoon in the Early Eocene: Evidence from the Gurha Mine, Rajasthan, India, *Palaeogeogr. Palaeoclimatol. Palaeoecol.*, 412, 187–198, <https://doi.org/10.1016/j.palaeo.2014.08.004>, 2014. Siler, N., Roe, G. H., Armour, K. C., and Feldl, N.: Revisiting the surface-energy-flux perspective on the sensitivity of global precipitation to climate change, *Clim. Dyn.*, 52, 3983–3995, <https://doi.org/10.1007/s00382-018-4359-0>, 2019. Slingo, J., Bates, P., Bauer, P., Belcher, S., Palmer, T., Stephens, G., Stevens, B., Stocker, T., and Teutsch, G.: Ambitious partnership needed for reliable climate prediction, *Nat. Clim. Change*, 12, 499–503, <https://doi.org/10.1038/s41558-022-01384-8>, 2022. Sluijs, A., Bijl, P. K., Schouten, S., Röhl, U., Reichert, G.-J., and Brinkhuis, H.: Southern ocean warming, sea level and hydrological change during the Paleocene-Eocene thermal maximum, *Clim Past*, 7, 47–61, <https://doi.org/10.5194/cp-7-47-2011>, 2011. Smith, F. A., Wing, S. L., and

Freeman, K. H.: Magnitude of the carbon isotope excursion at the Paleocene–Eocene thermal maximum: The role of plant community change, *Earth Planet. Sci. Lett.*, 262, 50–65, <https://doi.org/10.1016/j.epsl.2007.07.021>, 2007.

Smith, V., Warny, S., Jarzen, D. M., Demchuk, T., Vajda, V., and Gulick, S. P. S.: Paleocene–Eocene palynomorphs from the Chicxulub impact crater, Mexico. Part 2: angiosperm pollen, *Palynology*, 44, 489–519, <https://doi.org/10.1080/01916122.2019.1705417>, 2020.

Sniderman, J. M. K., Woodhead, J. D., Hellstrom, J., Jordan, G. J., Drysdale, R. N., Tyler, J. J., and Porch, N.: Pliocene reversal of late Neogene aridification, *Proc. Natl. Acad. Sci.*, 113, 1999–2004, <https://doi.org/10.1073/pnas.1520188113>, 2016.

Spicer, R. A., Yang, J., Spicer, T. E. V., and Farnsworth, A.: Woody dicot leaf traits as a palaeoclimate proxy: 100 years of development and application, *Palaeogeogr. Palaeoclimatol. Palaeoecol.*, 562, 110138, <https://doi.org/10.1016/j.palaeo.2020.110138>, 2021.

Su, T., Spicer, R. A., Wu, F.-X., Farnsworth, A., Huang, J., Rio, C. D., Deng, T., Ding, L., Deng, W.-Y.-D., Huang, Y.-J., Hughes, A., Jia, L.-B., Jin, J.-H., Li, S.-F., Liang, S.-Q., Liu, J., Liu, X.-Y., Sherlock, S., Spicer, T., Srivastava, G., Tang, H., Valdes, P., Wang, T.-X., Widdowson, M., Wu, M.-X., Xing, Y.-W., Xu, C.-L., Yang, J., Zhang, C., Zhang, S.-T., Zhang, X.-W., Zhao, F., and Zhou, Z.-K.: A Middle Eocene lowland humid subtropical “Shangri-La” ecosystem in central Tibet, *Proc. Natl. Acad. Sci.*, 117, 32989–32995, <https://doi.org/10.1073/pnas.2012647117>, 2020.

Suan, G., Popescu, S.-M., Suc, J.-P., Schnyder, J., Fauquette, S., Baudin, F., Yoon, D., Piepjohn, K., Sobolev, N. N., and Labrousse, L.: Subtropical climate conditions and mangrove growth in Arctic Siberia during the early Eocene, *Geology*, 45, 539–542, <https://doi.org/10.1130/G38547.1>, 2017.

Teodoridis, V., Mazouch, P., Spicer, R. A., and Uhl, D.: Refining CLAMP — Investigations towards improving the Climate Leaf Analysis Multivariate Program, *Palaeogeogr. Palaeoclimatol. Palaeoecol.*, 299, 39–48, <https://doi.org/10.1016/j.palaeo.2010.10.031>, 2011.

Tian, B. and Dong, X.: The Double-ITCZ Bias in CMIP3, CMIP5, and CMIP6 Models Based on Annual Mean Precipitation, *Geophys. Res. Lett.*, 47, e2020GL087232, <https://doi.org/10.1029/2020GL087232>, 2020.

Tripathi, S. K. M., Saxena, R. K., and Prasad, V.: Palynological investigation of the tura formation (early eocene) exposed along the tura-dalu road, west Garo Hills, Meghalaya, India, 2000.

Verma, P., Garg, R., Rao, M. R., and Bajpai, S.: Palynofloral diversity and palaeoenvironments of early Eocene Akri lignite succession, Kutch Basin, western India, *Palaeobiodiversity Palaeoenvironments*, <https://doi.org/10.1007/s12549-019-00388-1>, 2019.

Wang, H., Lu, H., Zhao, L., Zhang, H., Lei, F., and Wang, Y.: Asian monsoon rainfall variation during the Pliocene forced by global temperature change, *Nat. Commun.*, 10, 5272, <https://doi.org/10.1038/s41467-019-13338-4>, 2019.

West, C. K., Greenwood, D. R., and Basinger, J. F.: Was the Arctic Eocene ‘rainforest’ monsoonal? Estimates of seasonal precipitation from early Eocene megaflores from Ellesmere Island, Nunavut, *Earth Planet. Sci. Lett.*, 427, 18–30, <https://doi.org/10.1016/j.epsl.2015.06.036>, 2015.

West, C. K., Greenwood, D. R., Reichgelt, T., Lowe, A. J., Vachon, J. M., and Basinger, J. F.: Pa-

leobotanical proxies for early Eocene climates and ecosystems in northern North America from middle to high latitudes, *Clim. Past*, 16, 1387–1410, <https://doi.org/10.5194/cp-16-1387-2020>, 2020. Wiemann, M. C., Wheeler, E. A., Manchester, S. R., and Portier, K. M.: Dicotyledonous wood anatomical characters as predictors of climate, *Palaeogeogr. Palaeoclimatol. Palaeoecol.*, 139, 83–100, [https://doi.org/10.1016/S0031-0182\(97\)00100-4](https://doi.org/10.1016/S0031-0182(97)00100-4), 1998. Wilf, P., Wing, S. L., Greenwood, D. R., and Greenwood, C. L.: Using fossil leaves as paleoprecipitation indicators: An Eocene example, *Geology*, 26, 203–206, [https://doi.org/10.1130/0091-7613\(1998\)026<0203:UFLAPI>2.3.CO;2](https://doi.org/10.1130/0091-7613(1998)026<0203:UFLAPI>2.3.CO;2), 1998. Willard, D. A., Donders, T. H., Reichgelt, T., Greenwood, D. R., Sangiorgi, F., Peterse, F., Nierop, K. G. J., Frieling, J., Schouten, S., and Sluijs, A.: Arctic vegetation, temperature, and hydrology during Early Eocene transient global warming events, *Glob. Planet. Change*, 178, 139–152, <https://doi.org/10.1016/j.gloplacha.2019.04.012>, 2019. Williams, C. J. R., Lunt, D. J., Salzmann, U., Reichgelt, T., Inglis, G. N., Greenwood, D. R., Chan, W.-L., Abe-Ouchi, A., Donnadiou, Y., Hutchinson, D. K., de Boer, A. M., Ladant, J.-B., Morozova, P. A., Niezgodzki, I., Knorr, G., Steinig, S., Zhang, Z., Zhu, J., Huber, M., and Otto-Bliesner, B. L.: African Hydroclimate During the Early Eocene From the DeepMIP Simulations, *Paleoceanogr. Paleoclimatology*, 37, e2022PA004419, <https://doi.org/10.1029/2022PA004419>, 2022. Wing, S. L. and Greenwood, D. R.: Fossils and fossil climate: the case for equable continental interiors in the Eocene, *Philos. Trans. R. Soc. Lond. B. Biol. Sci.*, 341, 243–252, <https://doi.org/10.1098/rstb.1993.0109>, 1993. Wing, S. L., Herrera, F., Jaramillo, C. A., Gómez-Navarro, C., Wilf, P., and Labandeira, C. C.: Late Paleocene fossils from the Cerrejón Formation, Colombia, are the earliest record of Neotropical rainforest, *Proc. Natl. Acad. Sci.*, 106, 18627–18632, <https://doi.org/10.1073/pnas.0905130106>, 2009. Wolfe, J. A.: A Method of Obtaining Climatic Parameters from Leaf Assemblages, U.S. Government Printing Office, 360 pp., 1993. Wolfe, J. A.: Paleoclimatic Estimates from Tertiary Leaf Assemblages, *Annu. Rev. Earth Planet. Sci.*, 23, 119–142, <https://doi.org/10.1146/annurev.ea.23.050195.001003>, 1995. Xie, Y., Wu, F., Fang, X., Zhang, D., and Zhang, W.: Early Eocene southern China dominated by desert: Evidence from a palynological record of the Hengyang Basin, Hunan Province, *Glob. Planet. Change*, 195, 103320, <https://doi.org/10.1016/j.gloplacha.2020.103320>, 2020. Yang, J., Spicer, R. A., Spicer, T. E. V., Arens, N. C., Jacques, F. M. B., Su, T., Kennedy, E. M., Herman, A. B., Steart, D. C., Srivastava, G., Mehrotra, R. C., Valdes, P. J., Mehrotra, N. C., Zhou, Z.-K., and Lai, J.-S.: Leaf form–climate relationships on the global stage: an ensemble of characters, *Glob. Ecol. Biogeogr.*, 24, 1113–1125, <https://doi.org/10.1111/geb.12334>, 2015. Zhang, Y., Huck, T., Lique, C., Donnadiou, Y., Ladant, J.-B., Rabineau, M., and Aslanian, D.: Early Eocene vigorous ocean overturning and its contribution to a warm Southern Ocean, *Clim. Past*, 16, 1263–1283, <https://doi.org/10.5194/cp-16-1263-2020>, 2020. Zhu, J., Poulsen, C. J., and Tierney, J. E.: Simulation of Eocene extreme warmth and high climate sensitivity through cloud feedbacks, *Sci. Adv.*, 5, eaax1874, <https://doi.org/10.1126/sciadv.aax1874>, 2019.

Figures

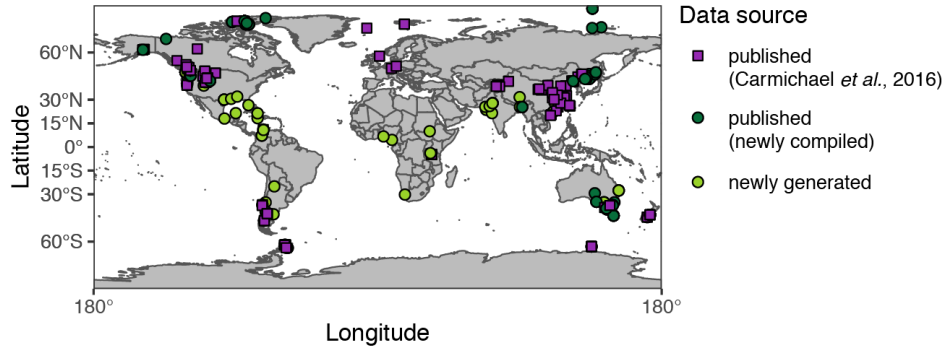


Figure 1. Overview of early Eocene precipitation proxy compilation. Previously published estimates compiled by the Carmichael *et al.*, (2016) shown as purple squares; additional published estimates plotted as dark green circles; new estimates (*this study*) plotted as light green circles. Sample locations plotted with their modern positions on a present-day world map.

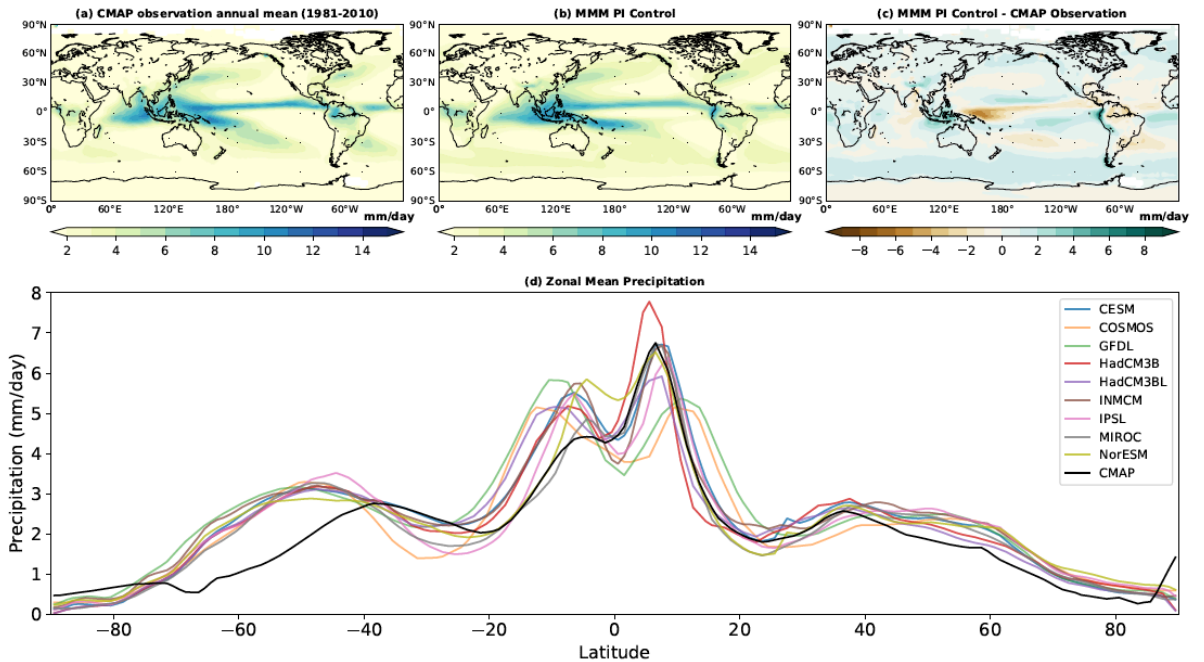


Figure 2. Rainfall patterns in DeepMIP pre-industrial simulations. a) Climate Prediction Center (CPC) Merged Analysis of Precipitation (CMAP) Observations (Xie & Arkin 1997), b) multi-model mean (MMM) of precipitation

estimates (mm/day) for the pre-industrial control runs for the 9 models in the DeepMIP ensemble (middle), **c**) MMM anomalies in precipitation (mm/day) for DeepMIP pre-industrial control runs minus modern observations. **d**) Zonal mean precipitation of DeepMIP model control runs and modern observations.

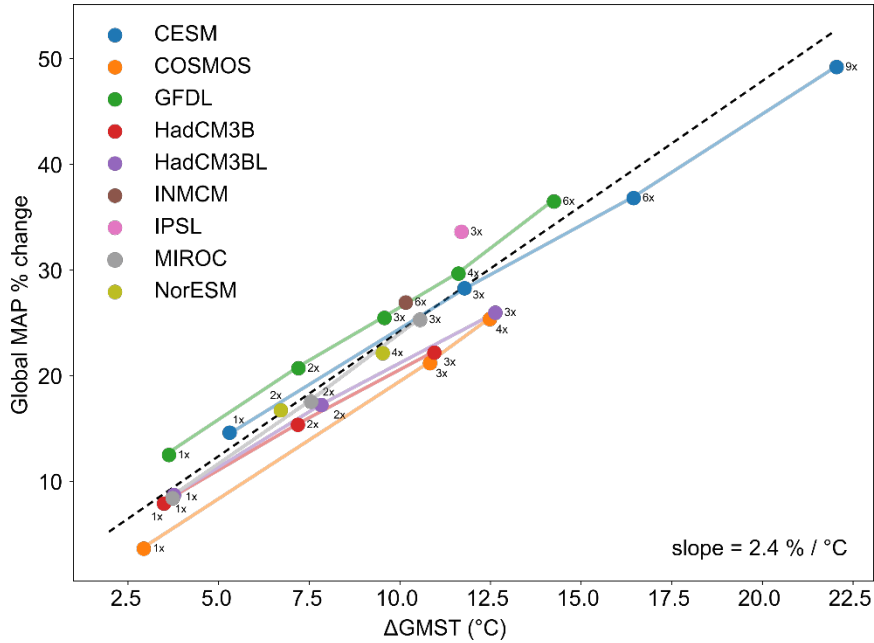


Figure 3. Global hydrological response to warming in the DeepMIP experiments. Global mean change in precipitation relative to pre-industrial (in % change) on the vertical axis plotted against global mean surface air temperature (GMST) relative to pre-industrial (in °C) on the horizontal axis. Simulations with the same model at three or more different CO₂ levels have been connected by coloured lines. Correlation coefficient of a linear fit through the combined values (black line) is 0.96, slope is 2.4% increase in precipitation per °C of warming.

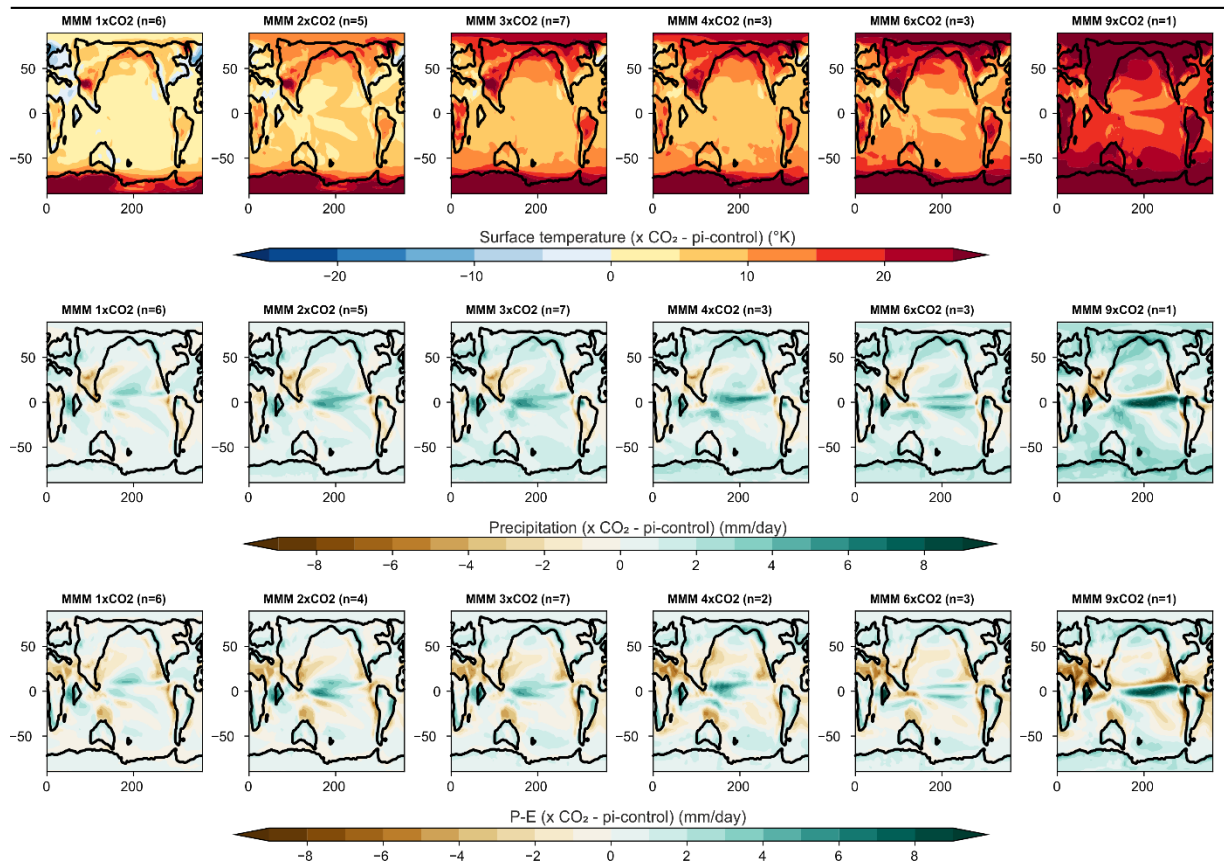


Figure 4. Multi-model mean temperature and precipitation anomalies relative to the pre-industrial period.

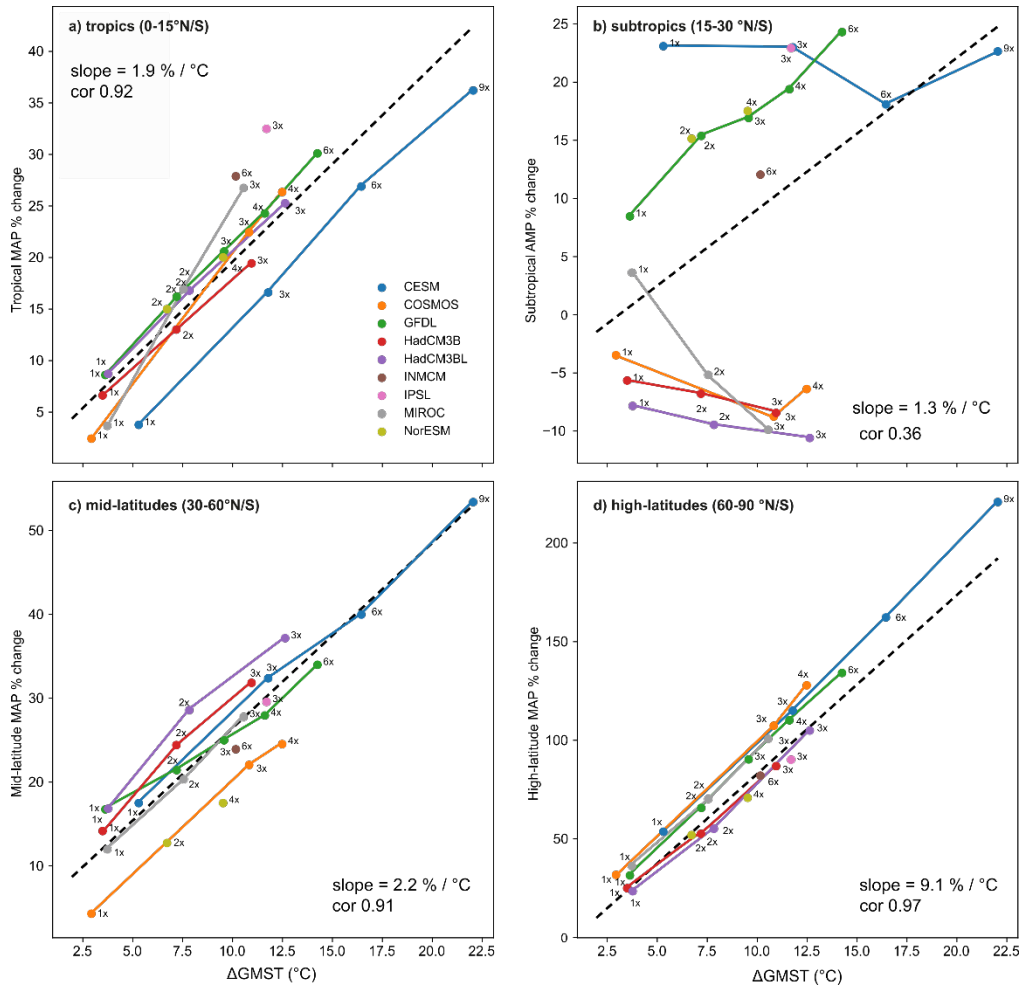


Figure 5. Zonally-averaged mean annual precipitation (MAP) values in the DeepMIP experiments for the a) tropics (15°–15° N/S), b) subtropics (15°–30° N/S), c) mid latitudes (30°–60° N/S), and d) high latitudes (60°–90° N/S). Panels (a-d) show the % change in MAP relative to pre-industrial vs the change in global mean surface air temperature change (GMST; °C) relative to pre-industrial. Simulations with the same model at 3 or more different CO₂ levels have been connected by colored lines. Dashed black line represents a linear fit through the combined values and the slope and correlation coefficient are shown in bottom right hand corner. Note that y-axis scaling differs between plots.

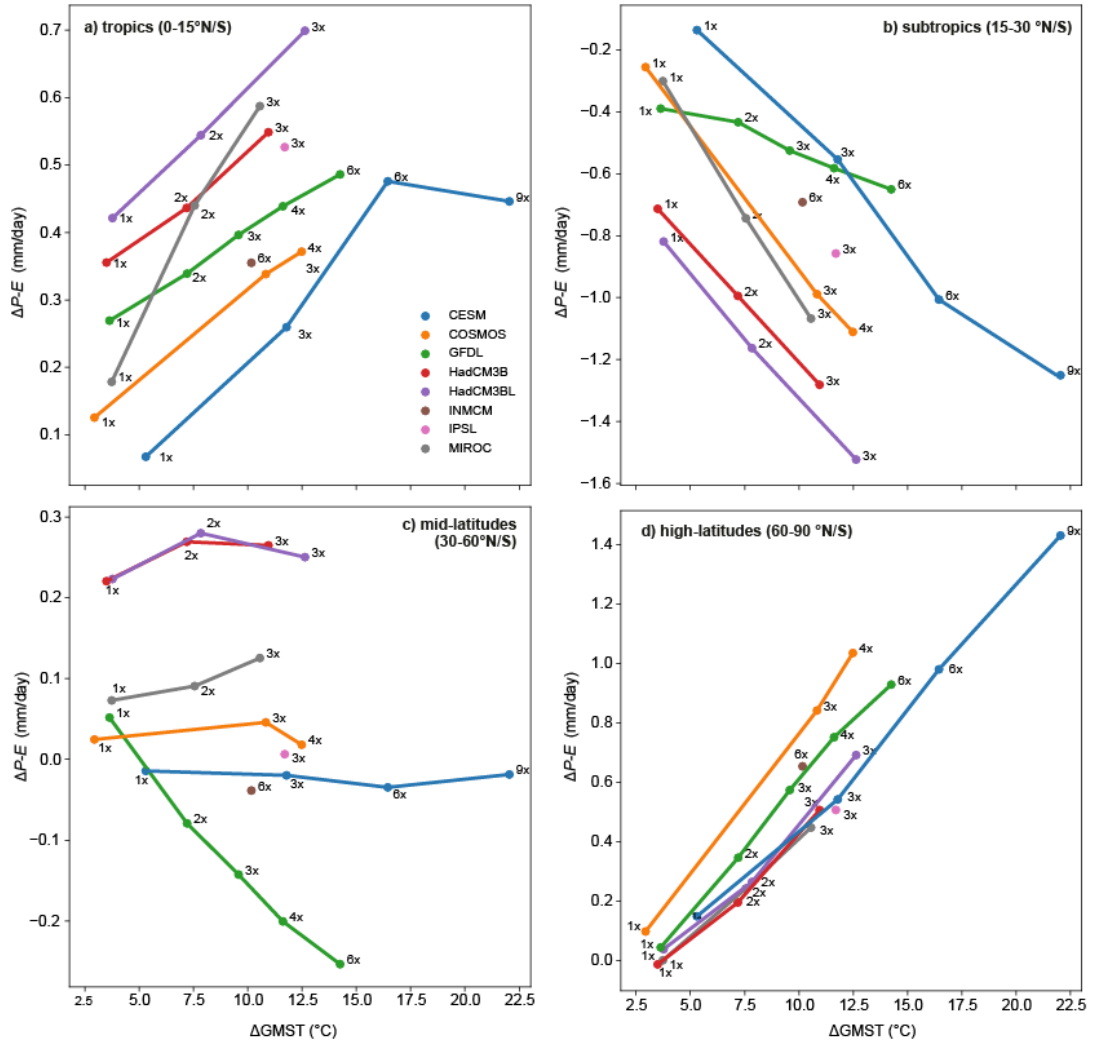
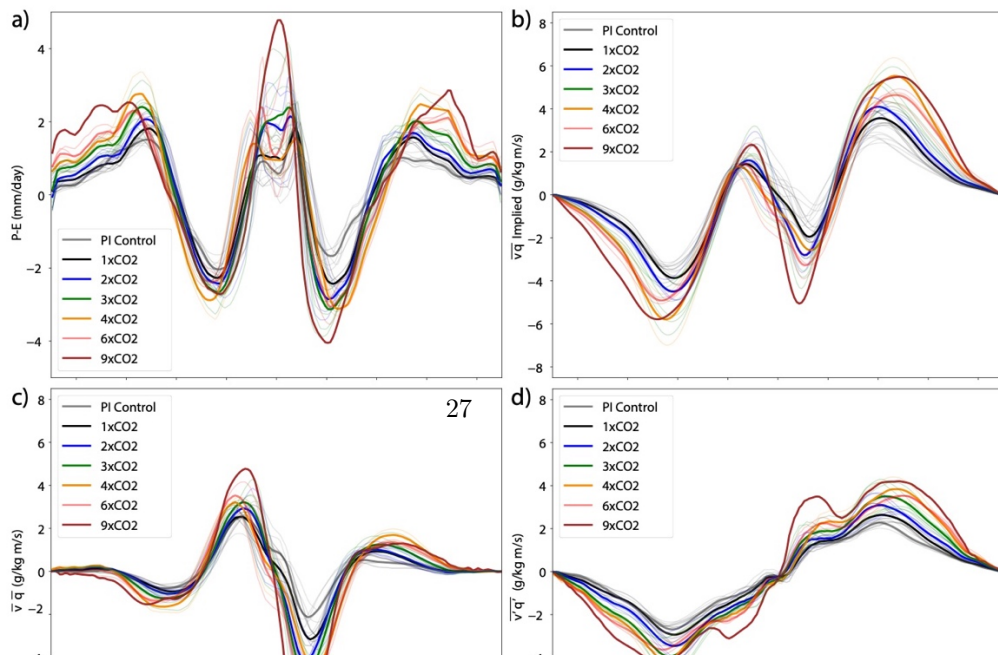
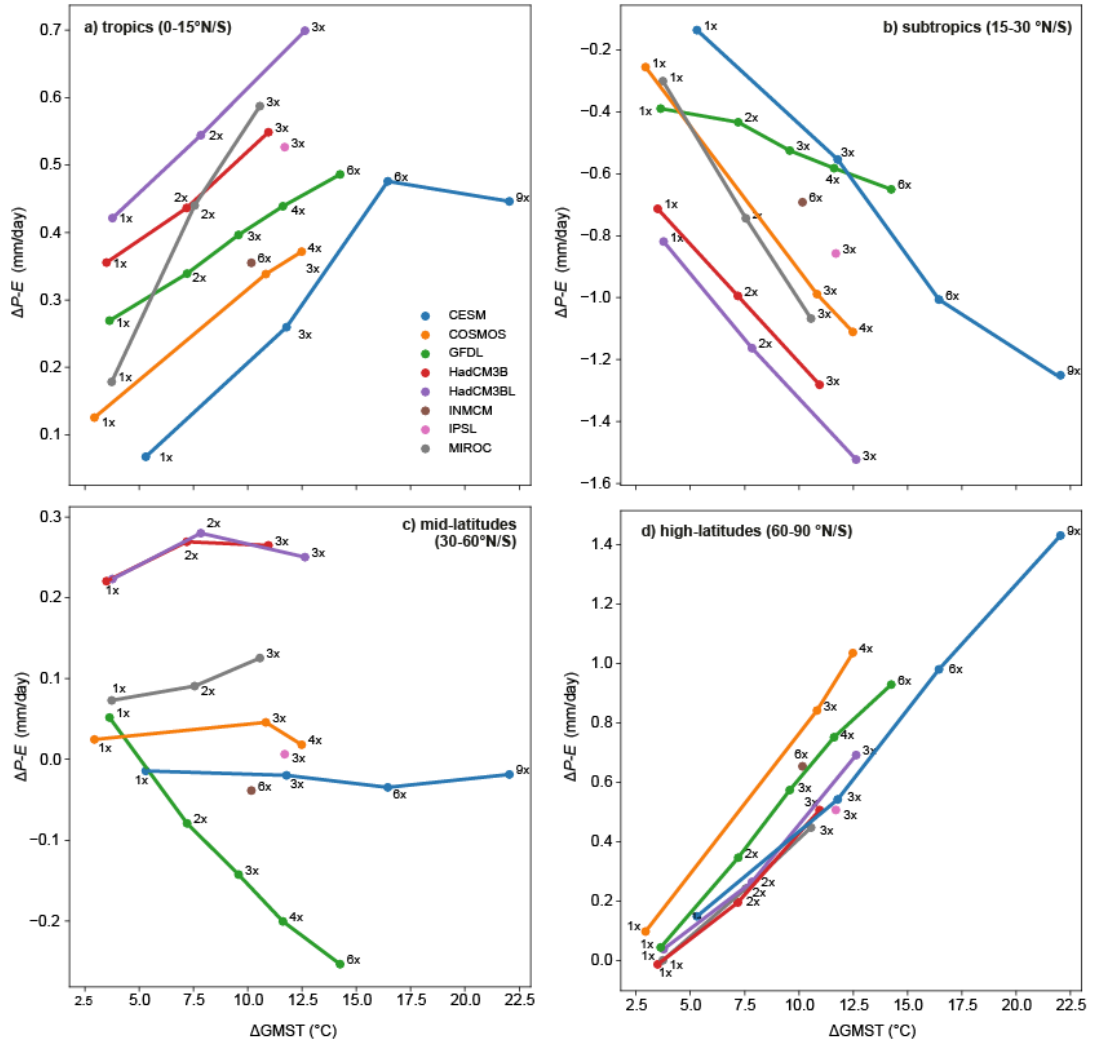


Figure 6. Zonally-averaged precipitation-evaporation ($P-E$) values in the DeepMIP model simulations.



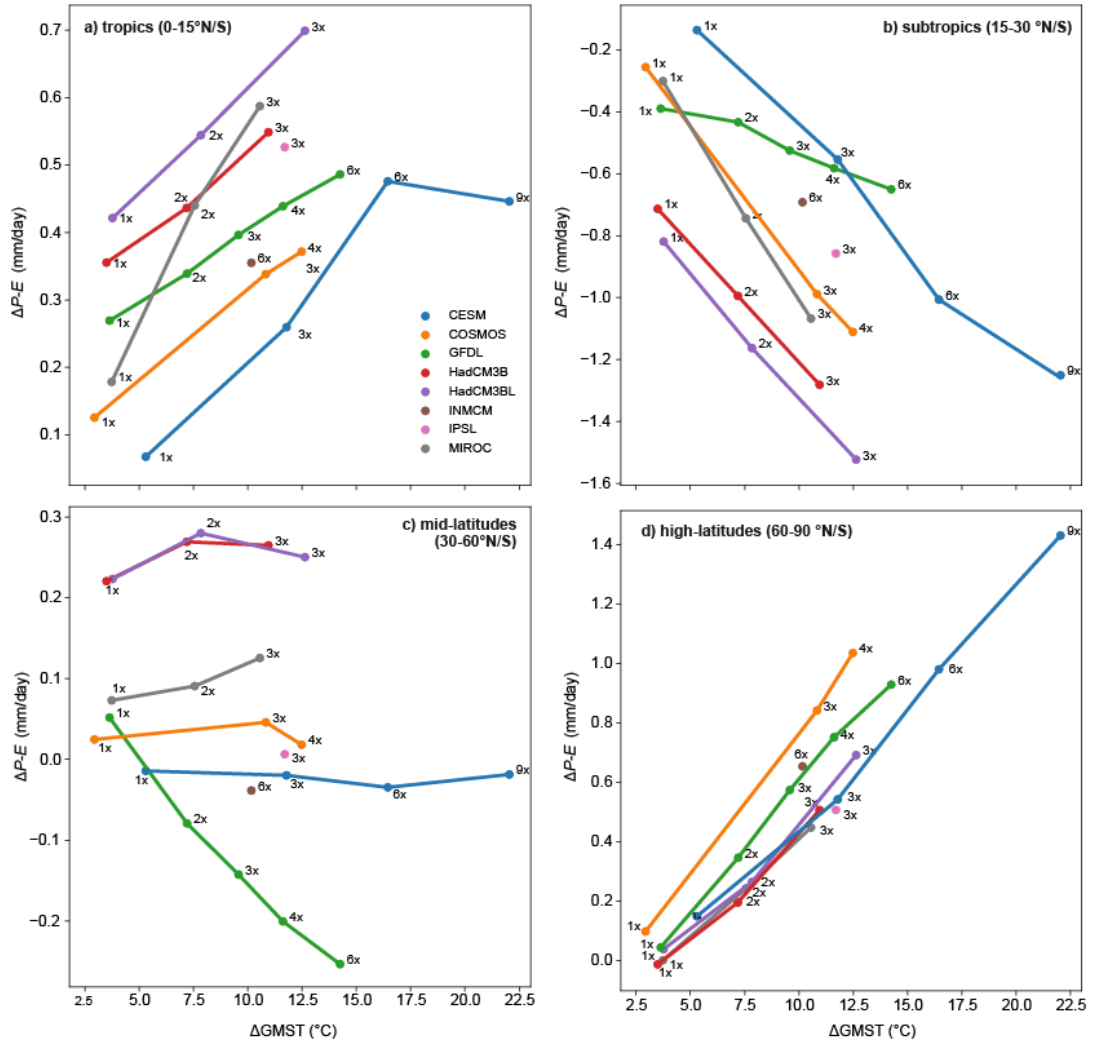


Figure 7. Zonal-mean components of the hydrological cycle as functions of latitude in the Deep

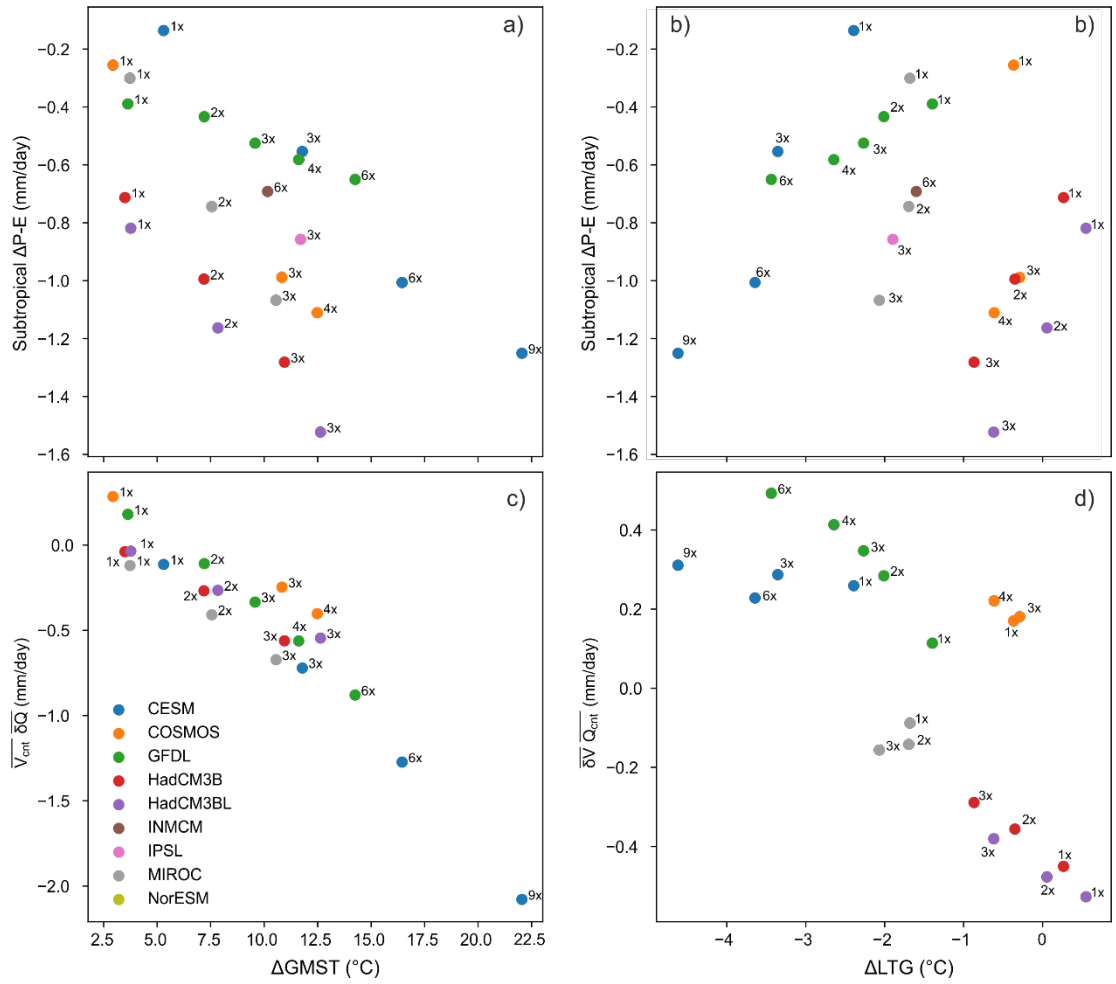


Figure 8. Moisture budget diagnostics show competing influence of humidity and atmospheric moisture

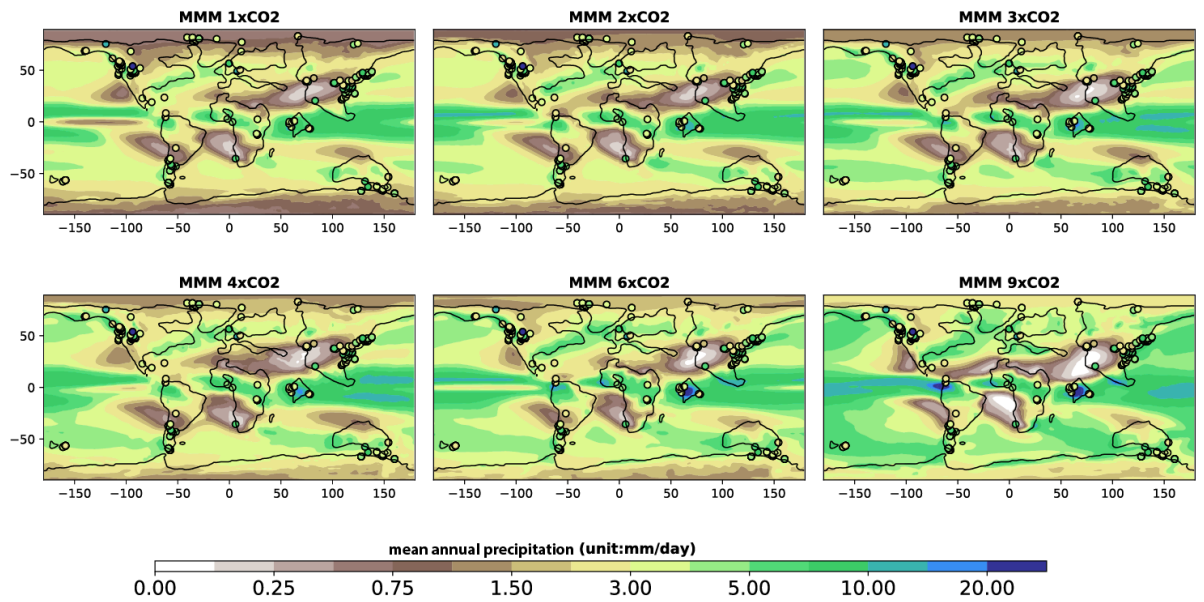


Figure 9. Map of proxy-based mean annual precipitation (MAP; mm/day) values. Plotted together with multi-model mean precipitation of the DeepMIP simulations.

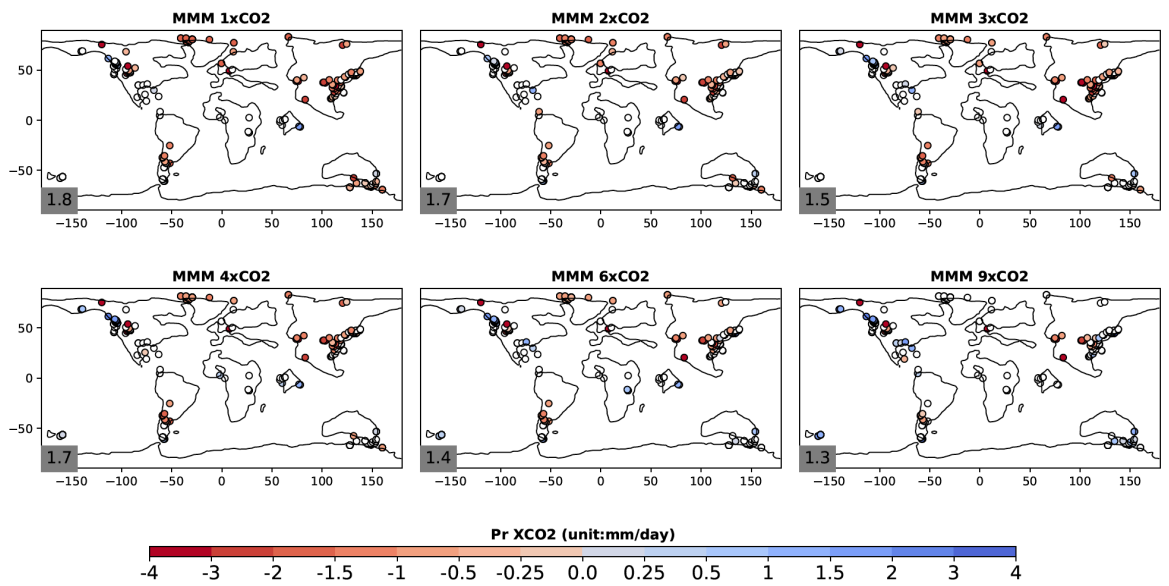


Figure 10. Data-model comparison for the early Eocene. In each panel, the early Eocene multi-model

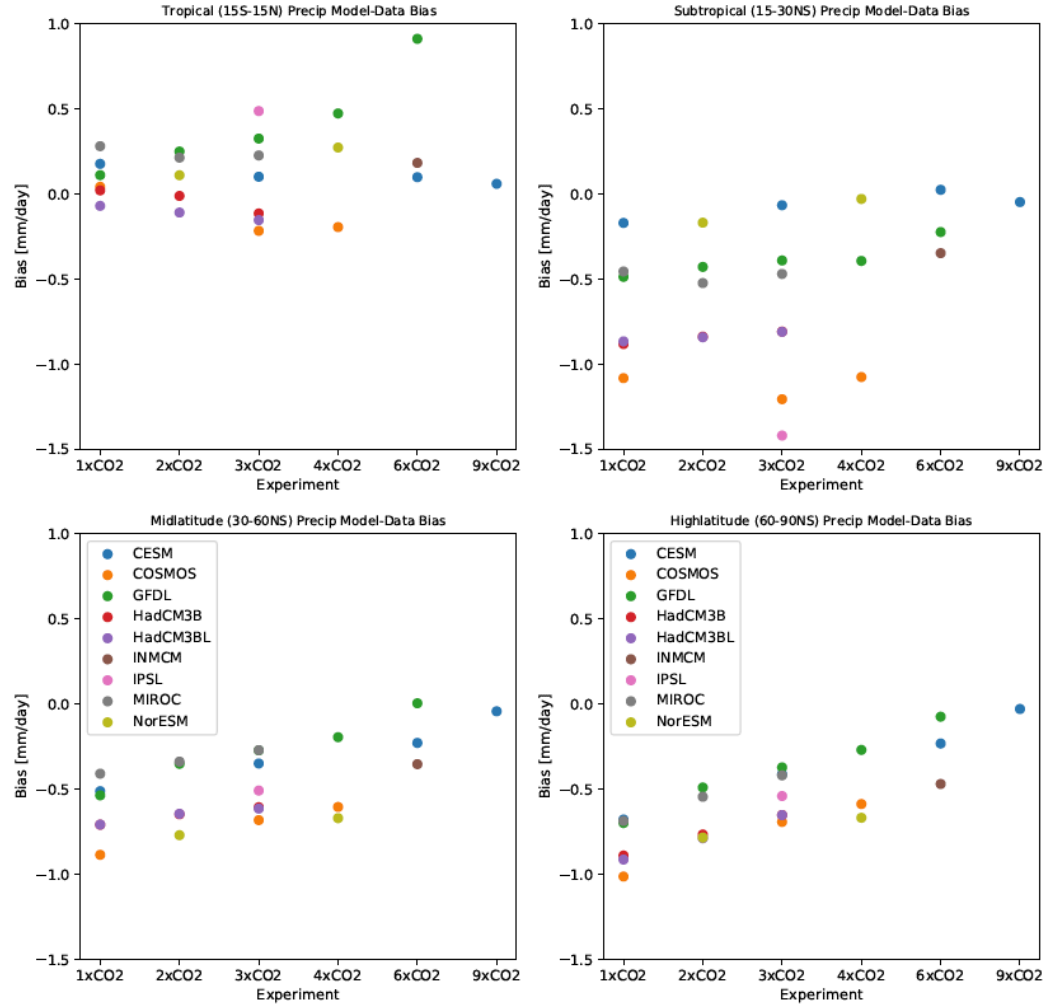


Figure 11. Zonally-averaged model-data mean annual precipitation (MAP) bias for the a) tropics (15° – 15° N/S), b) subtropics (15° – 30° N/S), c) mid latitudes (30° – 60° N/S), and d) high latitudes (60° – 90° N/S). Panels (a-d) show the model-data bias in mm/day for the different model simulations, sorted by CO_2 forcing.

Tables

Table 1. Overview of DeepMIP models and simulations, table adapted from Lunt et al., (2021).

Model	Long name	Short name	CO₂	CMIP generation	Simulation reference
CESM1.2_CAM5	Community Earth System Model	CESM	×1, ×3, ×6, ×9	CMIP5	Zhu et al., (2019)
COSMOS-landveg_r241	Community Earth System Models	COSMOS	×1, ×3, ×4	CMIP3	Lunt et al., (2021)
GFDL_CM2.3	Geophysical Fluid Dynamics Laboratory	GFDL	×1, ×2, ×3, ×4, ×6	CMIP3	Lunt et al., (2021)
HadCM3B_M2a1	Met Office Centre Climate Model	HadCM3	×1, ×2, ×3	CMIP3	Lunt et al., (2021)
INM-CM4-8		INMCM	×6	CMIP6	Lunt et al., (2021)
IPSLCM5A2	Institut Pierre Simon Laplace	IPSL	×1:5, ×3	CMIP5	Zhang et al., (2020)
MIROC4m	Model for Interdisciplinary Research on Climate	MIROC	×1, ×3	CMIP3	Lunt et al., (2021)
NorESM1_F	Norwegian Earth System Model	NorESM	×2, ×4	CMIP5-6	Lunt et al., (2021)